# **RESEARCH PAPER**

# Design, Optimization, and *in-Vitro* Evaluation of Dasatinib-Loaded Bilosomes Using Response Surface Methodology

Ahmed Hamed Salman 1,2 \*, Shaimaa Nazar Abd Alhammid 2

- <sup>1</sup> Department of Pharmacetics, College of Pharmacy, Al-Bayan University, Baghdad, Iraq
- <sup>2</sup> Department of Pharmaceutics, College of Pharmacy, University of Baghdad, Baghdad, Iraq

#### ARTICLE INFO

# Article History: Received 03 September 2025 Accepted 26 October 2025 Published 01 January 2026

Keywords:
Bile Salts
Cytotoxicity Tests
Dasatinib
Drug Delivery Systems
Nanoparticles
Solubility

# **ABSTRACT**

Dasatinib, a potent second-generation tyrosine kinase inhibitor for chronic myeloid leukemia (CML), exhibits pH-dependent solubility and poor oral bioavailability due to precipitation in the intestinal pH and extensive first-pass metabolism. Bilosomes, bile salt-stabilized nanovesicles, offer enhanced stability in the gastrointestinal tract and potential for improved oral delivery of poorly soluble drugs. To formulate and characterize an optimized oral bilosomal dasatinib system with improved physicochemical stability, dissolution behavior, and selective anticancer activity. Dasatinib-loaded bilosomes were prepared using reverse-phase evaporation and optimized via a Box-Behnken design, varying Span 60, Tween 60, cholesterol, sodium deoxycholate, and Soluplus. The optimized formulation underwent characterization (particle size, PDI, zeta potential, entrapment efficiency, TEM), and solid-state analysis (FTIR, DSC, XRD). In vitro release studies at pH 1.2, 6.8, and 7.4 were fitted to kinetic models. Cytotoxicity was assessed in K562 CML cells and normal human lymphocytes using the MTT assay. The optimized bilosomes (113.2 nm, PDI 0.109, zeta potential -22.36 mV, EE 81.02%) showed spherical morphology and amorphous drug dispersion. Compared to pure drug, release was sustained with significantly higher dissolution at intestinal pH, best fitting the Korsmeyer-Peppas model at pH 6.8/7.4. Cytotoxicity studies revealed potent activity against K562 cells (IC<sub>50</sub> = 1.308 ng/mL) with ~17.6-fold selectivity over normal lymphocytes. The developed bilosomal system effectively encapsulated dasatinib, enhanced stability, modulated release, and achieved selective in vitro anticancer activity, supporting its potential as a promising oral delivery platform for CML therapy.

# How to cite this article

Salman A., Abd Alhammid S. Design, Optimization, and in-Vitro Evaluation of Dasatinib-Loaded Bilosomes Using Response Surface Methodology. J Nanostruct, 2026; 16(1):109-133. DOI: 10.22052/JNS.2026.01.012

# INTRODUCTION

Dasatinib monohydrate (DST) is a secondgeneration tyrosine kinase inhibitor (TKI) indicated for patients with chronic myeloid leukemia (CML) who exhibit resistance or intolerance to prior therapies. It effectively inhibits BCR/ABL and SRC-family kinases, in addition to c-KIT, PDGFR- $\alpha$  and - $\beta$ , and ephrin receptor kinase [1]. Aqueous solubility is believed to contribute substantially to variability in medication absorption [2]. DST is rapidly absorbed, achieving peak plasma concentrations within 0.5 to 3 hours post-oral

<sup>\*</sup> Corresponding Author Email: ahmed.s@albayan.edu.iq

dosing, with solubility contingent upon pH levels [3]. The inadequate bioavailability of DST may be attributed to its limited solubility in aqueous environments, as it is categorized as BCS class II. The bioavailability of BCS class II medicines is based on solubility and dissolution [4].

In vitro findings demonstrate a pH-dependent solubility of DST. Solubility diminishes significantly at pH levels over 4.0, declining from 18.4 mg/ mL at pH 2.6 to 0.205 mg/mL at pH 4.28, and further to <0.001 mg/mL at pH 6.99 [5]. Thus, considerable pharmacokinetic interactions have also been reported between TKIs and medications that elevate stomach pH. The co-administration of DST with famotidine and antacids resulted in a decrease in AUC of around 60% and 55%, respectively [5]. A similar interaction was reported with omeprazole [6]. Consequently, H2 antagonists and proton pump inhibitors are not advised for simultaneous administration with dasatinib monohydrate [7]. In addition to medication interactions, reduced absorption of dasatinib may occur under pathophysiological conditions that elevate stomach pH, such as hypochlorhydria or achlorhydria, which is prevalent in the population, with its incidence rising with age [8]. Overcoming such shortcomings has gained attention in recent years to improve the oral bioavailability of DST. One of these attempts was to use amorphous solid dispersion (ASD) [9-11], nanoemulsifying drug delivery system [12], nanoparticles [13, 14].

Bilosomes, which are vesicles stabilized by bile salts, constitute a novel vesicular carrier [15]. They function as closed vesicles comprised of nonionic surfactants that resemble niosomes but incorporate bile salts [16]. When taken orally, bilosomes offer protection against challenging circumstances, including the stomach's acidic environment and digestive enzymes, due to the inclusion of bile salts as their primary structural component [17]. Moreover, they provide superior durability against the challenging environments of the gastrointestinal tract for the encapsulated therapeutic agent, in contrast to conventional niosomes and liposomes, which rapidly degrade and release the encapsulated medication before reaching the target cells [18]. Bilosomes exhibit remarkable durability at ambient temperatures and within refrigeration, primarily due to the large negative charge conferred by bile salts. From a commercial perspective, bilosomes may be favored over alternative nanocarrier systems because

of their accessibility and the simplicity and costeffectiveness of their manufacturing processes. Moreover, this approach offers improved patient adherence [19-21]. Based on these properties, bilosomes were utilized to deliver DST, thereby improving solubility and enhancing delivery through the gastrointestinal tract (GIT).

Bilosomes primarily consist of phospholipids (in liposomes) or nonionic surfactants (in niosomes), cholesterol, and bile salts. The ratios of these substances vary according to the characteristics of the encapsulated medicine and the desired method of administration. The structural components are essential for the effective production of bilosomes with the requisite properties [22].

#### **MATERIALS AND METHODS**

Materials

The materials employed in this study include cholesterol from Avonchem, UK; methanol (99%) from CHEM-lab, Belgium; mannitol; potassium dihydrogen phosphate, phosphate-buffered saline (pH 7.4), and sodium hydroxide, all sourced from Hi-Media, India; and sodium deoxycholate from Avonchem Ltd., UK; Triton-X100 purchased from Loba Chemie Pvt. Ltd., India.

Additional reagents comprise Span® surfactants 20, 40, 60, and 80, as well as Tween® surfactants 20, 40, 60, and 80, both from Loba Chemie Pvt. Ltd., India; dasatinib monohydrate powder from Wuhan Hanweishi Pharmchem Co., China; Soloplus® from Germany; and ethanol (96%), dimethyl formamide, and hydrochloric acid (HCl), all provided by CHEM-lab, Belgium.

# Characterization of dasatinib

Preformulation studies are conducted to evaluate the physicochemical characteristics of the medication and excipients, which may impact the effectiveness and formulation of dosage forms. Such knowledge can be utilized as a rationale for developing new items or asserting that existing ones necessitate molecular modifications [23].

# Determination of Absorption Maxima ( $\lambda_{max}$ )

The UV spectra were acquired using a double-beam UV/Visible spectrophotometer (Shimadzu UV-19001, Japan) with 10 mm matched quartz cells. The solution contains 100 mg of the drug per 100 mL dissolved in different solutions [24]. The calibration curve is illustrated in Supplementary file S1 (Fig. S1).

J Nanostruct 16(1): 109-133, Winter 2026



Solubility of dasatinib in different vehicles

The solubility of dasatinib in various solvents was determined using the saturation-solubility method, in which 10 mg of dasatinib was placed into a clean and dry 10 mL volumetric flask, and the resulting volume was documented [25]. 10 mL of each solvent, including deionized water, phosphate buffer (pH 6.8), phosphate buffer saline (pH 7.4), 0.1 N HCl, phosphate buffer (pH 6.8) containing Triton-X100, and phosphate buffer saline (pH 7.4) containing Triton-X100, were used to fill the flask; after agitating the flask and allowing it to rest momentarily. The solution was placed in a water bath shaker for 48 hours at 37 °C. Afterward, the solution was centrifuged (6,000 RPM for 15 minutes), and the supernatants were filtered through a 0.22-micron syringe filter. The solubility was determined by using a UV-spectrophotometer [26].

Pilot study for the initial selection of surfactants for dasatinib-loaded bilosomes Formulation

The reverse-phase evaporation method was used to formulate the DST-LB formulas; the components of DST-LB must include cholesterol, nonionic surfactant (Tweens and spans), bile salts (sodium deoxycholate (DSC)), and stabilizing agents (soluplus) [27, 28].

The dasatinib-loaded bilosome formulas were prepared using the reverse-phase evaporation method with some modifications [29]. The details of the procedure are as follows: a mixture of surfactants (Tween 60 and Span 60), a specific amount of cholesterol, and 20 mg of dasatinib were combined in a round-bottom flask with an adapter containing 10 mL of ethanol. The solution

was sonicated in a water bath sonicator (Copley Scientific Limited, Nottingham, England) at 40°C for 15 minutes, ensuring the solubilization of the mixture. The aqueous phase solution was made by dissolving a measured amount of bile salts (SDC) and Soluplus in 5 mL of deionized water. The phases were mixed using an ultrasonic bath (Copley Scientific Limited, Nottingham, England) to form a stable white emulsion. The emulsion was then dried using a rotary evaporator at 150 rpm (150 mbar at 40 °C for 60 minutes) to form a thin film and rehydrated with 10 mL deionized water. The resulting bilosome dispersion (2 mg/mL) was heated in a water bath sonicator (Copley Scientific Limited, Nottingham, England) at 40°C for 30 minutes to create a homogeneous dispersion, followed by sonication (VCX 750, VibraCell™ Sonicator, Sonics and Materials Inc., USA) for 5 minutes at 30% amplitude with a pulse of 10 seconds on and 10 seconds off. This process was used to reduce vesicle size, and the dispersion was then stored at 4°C for further analysis.

Initially, to choose the best nonionic surfactant from various concentrations of Tweens (20, 40, 60, and 80) and Spans (20, 40, 60, and 80), a pilot study was done based on 25 formulas while using fixed concentrations of cholesterol, DSC, and soluplus (Supplementary file S2, Tables S1, and S2). The particle size (PS), polydispersity index (PDI), and entrapment efficacy (EE) of the resulting formulas were the selected parameters to choose the best formula.

Preparation of dasatinib-loaded bilosomes (DST-LB) formulas

The second formulation step involved using the

$$Y = \beta_0 + \beta_1 x_1 + \beta_2 x_2 + \beta_3 x_3 + \beta_4 x_4 + \beta_5 x_5 + \beta_{11} x_1^2 + \beta_{22} x_2^2 + \beta_{33} x_3^2 + \beta_{44} x_4^2 + \beta_{55} x_5^2 + \beta_{12} x_1 x_2 + \beta_{13} x_1 x_3$$
(1)  
+ \(\beta\_1 4 x\_1 x\_4 + \beta\_{15} x\_1 x\_5 + \beta\_{23} x\_2 x\_3 + \beta\_{24} x\_2 x\_4 + \beta\_{25} x\_2 x\_5 + \beta\_{34} x\_3 x\_4 + \beta\_{35} x\_3 x\_5 + \beta\_{45} x\_4 x\_5 \)

Medium Low High **Factors** Independent variables (-1)(0)(+1) $X_1$ Cholesterol 60 120 180 mg Χz Tween 60 50 150 mg  $\chi_3$ Span 60 100 200 300 mg X4 SDC mg 5 10 15 X5 Soluplus 50 75 100 mg Response  $Y_1$ Particle Diameter mm  $Y_2$ PDI % Encapsulation Efficiency (EE) %  $Y_3$ 

Table 1. Independent and dependent variables applied in a Box-Behnken design.

Box-Behnken design to optimize the Tween 60, Span 60, cholesterol, DSC, and Soluplus, resulting in 46 formulas. The resulting formulas, PS, PDI, EE, and the in vitro release study for the optimal formula, were the parameters used to choose the optimized DST-LB formula. The Box-Behnken statistical design with five factors (3<sup>5</sup>), three levels (-1, 0, 1), and 45 runs was chosen for the optimization analysis. The experimental design theoretically consists of points at the midpoint of each edge and the replicated center point of the multidimensional cube.

The dependent and independent variables in the experimental design of the D-LB, formulated with cholesterol, Span 60, Tween 60, SDC, and Soluplus, are presented in Table 1. Using the software Minitab\* 17.1.0, the following equation (quadratic model) was applied for designing the different formulae (Eq. 1).

The goal of exploring the optimized formula DST-LP included setting PS (Y1) to a target of 100 nm, PDI (Y2) to a target of 0.2%, and EE (Y3) to a target of  $\leq$ 0.8.

All batches of the formulations were produced as scheduled and evaluated for varied responses. The current study employed ANOVA (Analysis of Variance) to examine each variable individually and in conjunction with other responses to enhance the outcomes. The Box-Behnken Design was employed, and outcomes were examined and validated using a significant coefficient with R2 values throughout the entire experimental region. Furthermore, optimal checkpoint formulations were developed and assessed to identify the optimized formula for the specified experimental domain and equations [30].

Characterization of dasatinib-loaded bilosomes formulation

Measurement of particle size, polydispersity index, and zeta potential

Dynamic light scattering (DLS) was used to determine the polydispersity index (PDI) and polydispersity of DST-LB using a Zetasizer (Malvern, UK). The measurements were conducted at 25±2°C [28]. Additionally, the zeta potential (ZP) of the

bilosomes was measured by observing how the bilosomes moved in an electrical field in deionized water using the same instrument. To ensure accurate measurements, the samples were diluted 10-fold with deionized water before analysis. The ZP measurement allowed an understanding of the surface charge of the bilosomes, which was important for the stability of the bilosomes [31].

#### **Drug Content Determination**

An exact volume of 1 mL, equivalent to 1.33 mg of dasatinib, was measured and mixed with 9 mL of DMF. The mixture was then sonicated in a sonication bath for 5 min. 1 mL was taken from this prepared solution and further diluted with 100 mL DMF [32].

The resulting solution was analyzed for drug content using a UV/VIS spectrophotometer at the specified  $\lambda_{\text{max}}$ . The percentage of drug content in the bilosomes was calculated using the Eq. 2.

Determination of percentage entrapment efficiency

The direct method (dialysis method) was used to calculate the EE; a 2 mL DST-LB formula was placed in a dialysis bag (HiMedia Laboratories LLC, USA) and dialyzed against 500 mL of medium (deionized water + 0.5% Triton X). After 24 hours, the amount of drug recovered from the dialysis bag (Wr) was determined by UV-vis spectroscopy. The EE was calculated using the Eq. 3 [33]:

$$EE(\%) = \frac{W_r}{W_{total}} \times 100\% \tag{3}$$

Where  $W_{total}$  is the total amount of drug in the dialysis bag before the procedure,  $W_r$  is the amount of drug that was recovered from the dialysis bag at the end.

*In vitro study of the drug release* 

The dialysis bag method was used to assess the drug release from DST-LB using a dialysis membrane. A dialysis bag containing 1 mL of a different formulation was placed in 900 mL

Drug content (%) = 
$$\frac{\text{Measured amount of dasatinib}}{\text{Theoretical amont of dasatinib}} \times 100$$
 (2)

of various media (phosphate buffer (pH 6.8) containing Triton-X100, and phosphate-buffered saline (pH 7.4) containing Triton-X100, 0.1 N HCl) and maintained at 37±0.5°C and 75 rpm using a USP apparatus II (paddle). For the media at pH of 6.8 and 7.4, the samples (5 mL) were taken after regular intervals (10, 20, 30, 60, 90, 120, 180, 240, 300, 360, 420, 480, 540, and 600 minutes), meanwhile at pH 1.2 the time interval was (5, 10, 15, 20, 30, 45, 60, 90, and 120 minutes) and measured using UV spectrophotometry at the specified  $\lambda_{\text{max}}$ . The dialysis bag method releases the drug from the bilosomes into the buffer medium. The samples were then taken and measured for drug concentration over time to determine the release profile of the drug from the bilosomes

#### Dissolution kinetics model profile

The data acquired from the in vitro investigation were analyzed using various mathematical equations that accurately represent the kinetics and mechanism of dasatinib leakage from the chosen BL formula. DDsolver, an additional tool in Microsoft Excel, facilitated this analysis [35]. The kinetic models are presented in Table 2. The correlation of determination (R²) can be utilized to pick the most appropriate model among the regression models with equal parameters [36].

# Mechanism of release

The dissolution kinetics were assessed using model-dependent approaches with DDSolver® [35]. The Korsmeyer-Peppas approach is used to investigate the mechanism of active ingredient leakage from polymeric formulations when the leakage mechanism is not well understood or when multiple models of leakage phenomena are involved. The diffusional exponent (n) determined by Korsmeyer-Peppas is crucial for calculating the drug's 60% leakage; (N<0.45) Fickian diffusion mechanism, (0.45<N<0.89) non-Fickian transport, (N = 0.89) Case II transport, and (N>0.89) super Case II transport [36, 37].

# Lyophilization of the optimized formula

Lyophilization of the optimized bilosomes formula was performed using mannitol as a cryoprotectant (1 w/v%). The lyophilization process involved subjecting the formulation to a primary freezing temperature of -20 °C for 24 hours, followed by immersion in liquid nitrogen

for 15 minutes. Subsequently, the formulation was lyophilized for 72 hours under a pressure of 0.4 bar [38]. The obtained powder was stored in a tightly closed container for further investigations.

# Differential Scanning Calorimeter (DSC) Analysis

The DSC (DSC-60 Plus, Shimadzu, Japan) measurements were conducted utilizing an aluminum-sealed plate in a nitrogen environment. The scans were obtained within a temperature range of 30 to 300 °C, with a consistent heating rate of 10 °C/min, while being scanned at a constant flow rate of 50 mL/min. Heat flow vs. temperature (thermograms) was recorded [39].

# Fourier-Transform Infrared Spectroscopy (FTIR)

The FT-IR spectra (Shimadzu 8300, Japan) were obtained by grinding dasatinib with KBr and preparing discs under compressed pressure, at a ratio of 1:100 (drug: KBr). The spectra were obtained by averaging 32 scans of the fused discs in the spectral region of 4000-400 cm<sup>-1</sup>, with a resolution of 4 cm<sup>-1</sup> [40-42]. Each sample was analyzed in triplicate.

#### Powder X-ray Diffraction (P-XRD) Analysis

The XRPD patterns were obtained at ambient temperature using the Shimadzu (XRD-6000, Japan) diffractometer equipped with an imaging plate area detector and graphite monochromated with Cu-K $\alpha$  radiation ( $\lambda$  = 1.5406 Å), operating at 40 kV and 30 mA. The 2-theta range spanned from 10 to 80 degrees, receiving slit 0.3 mm, scan speed 10 deg/min, sampling pitch 0.04 deg, and preset time 0.24 sec [39, 41].

Furthermore, crystallinity index (CI) was calculated using OriginPro, Version 2024. OriginLab Corporation, Northampton, MA, USA. In which the Total area of the crystalline peaks was divided by the Total area of the crystalline and amorphous peaks [43, 44].

# Transmission Electron Microscopy (TEM)

Zeiss Libra 120 PLUS (Carl Zeiss NTS, Germany) was used for all TEM investigations of bilosome morphology and bilayer architecture. A freshly prepared optimized bilosome suspension was diluted with deionized water (1 mg/mL), and then the suspension was filtered. The diluted suspension was sonicated for 5 minutes in an ice-cooled bath to disperse aggregates and maintained on ice until grid deposition. Continuous carbon-coated,

200-mesh copper grids were glow-discharged (15 mA, 30 s) to render the surface hydrophilic. A 3  $\mu$ L aliquot of nanobilosome suspension was applied and adsorbed for 60 s. Excess liquid was wicked away with filter paper. Then, 5  $\mu$ L of 2% (w/v) uranyl acetate (pH 4.5) was added for 30 s. Grids were blotted, air-dried under dust-free conditions for 10 min, and loaded immediately into the microscope. Digital micrographs were recorded with minimal beam dose to prevent radiation damage. Five randomly selected grid squares were imaged per

sample to ensure representative morphology [45].

In vivo study

K562 – Human Chronic Myelogenous Leukemia Cell Line

The human myeloid leukemia cell line K562 was obtained from ATCC-USA. The cells were cultured in RPMI-1640 medium supplemented with 10% (v/v) heat-inactivated fetal bovine serum (Gibco), 100 IU/mL penicillin, 100  $\mu$ g/mL streptomycin, 2 mM L-glutamine, and 10 mM HEPES buffer.

Mean Optical Density (OD) = 
$$\frac{(OD_1 + OD_2 + OD_3)}{3}$$
 (4)

Cell Viability (%) = 
$$\left(\frac{\text{Mean OD of Treated Sample}}{\text{Mean OD of Control}}\right) * 100$$
 (5)

Percentage Growth Inhibition (Cytotoxicity) = 100 - Viability

(6)

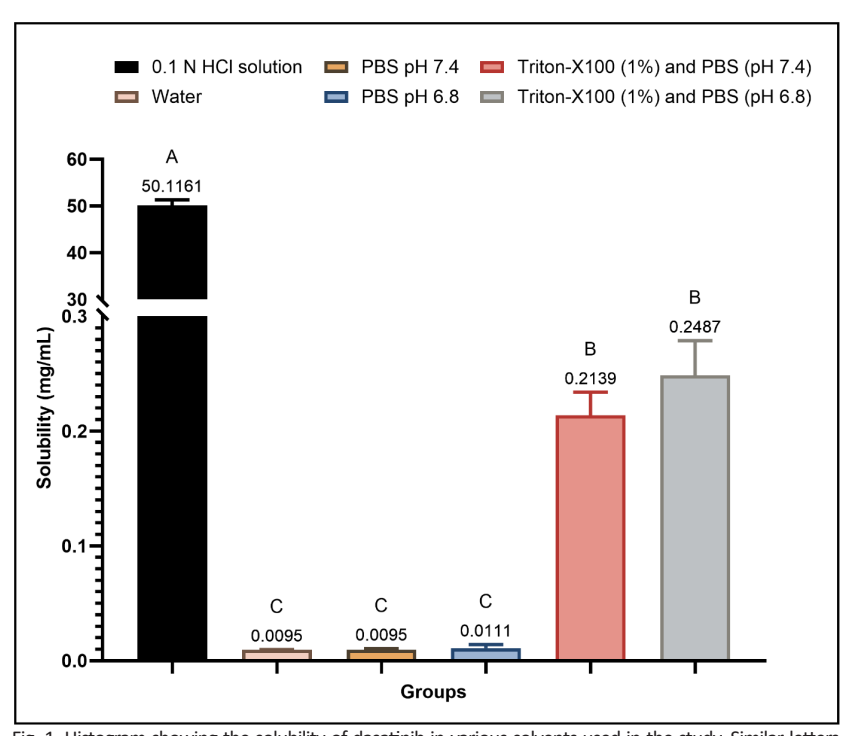


Fig. 1. Histogram showing the solubility of dasatinib in various solvents used in the study. Similar letters indicate no significant difference (A vs. B, or C indicates p-value<0.05, B vs. C indicates p-value <0.05). Brown-Forsythe ANOVA test with post hoc Dunnett's T3 multiple comparisons test was used.

Table 2. Experimental design and response of D-LB.

F	Span 60	Tween 60	Cholesterol	SDC	Soluplus	PS	PDI	EE%
1	300	100	120	10	50	291±1.746	0.3±0.004	0.91±0.006
2	200	100	120	10	75	89.8±1.527	0.23±0.003	0.82±0.014
3	100	100	180	10	75	111.3±0.557	0.08±0.000	0.79±0.009
4	200	100	120	15	100	151.8±1.670	0.29±0.006	0.85±0.006
5	100	150	120	10	75	106.2±1.381	0.26±0.002	0.82±0.009
6	300	100	120	10	100	268.1±5.094	0.49±0.006	0.92±0.013
7	100	100	120	10	100	139.1±1.947	0.35±0.002	0.76±0.013
8	100	50	120	10	75	205.3±2.874	0.33±0.002	0.77±0.008
9	100	100	120	5	75	175.5±2.984	0.24±0.004	0.8±0.006
10	200	50	60	10	75	172.8±1.901	0.41±0.006	0.73±0.004
11	200	150	180	10	75	97.1±1.262	0.05±0.001	0.82±0.014
12	100	100	120	10	50	123.3±1.356	0.47±0.003	0.75±0.012
13	200	100	120	10	75	94±1.410	0.12±0.002	0.83±0.005
14	200	50	120	10	50	139.1±2.226	0.35±0.003	0.78±0.004
15	200	50	120	10	100	184.3±2.765	0.25±0.004	0.76±0.004
16	200	50	120	15	75	271.3±1.899	0.38±0.004	0.70±0.008
17	200	100	180	10	50	275.5±3.031	0.31±0.005	0.89±0.009
18	200	100	180	10	100	211.8±3.601	0.43±0.006	0.88±0.012
19	200	150	120	15	75	139.1±0.835	0.35±0.005	0.84±0.004
20	200	150	60	10	75	111.6±2.009	0.37±0.006	0.84±0.017
21	100	100	60	10	75	101.4±1.014	0.21±0.003	0.78±0.004
22	200	100	180	5	75	255.4±3.831	0.46±0.005	0.87±0.007
23	200	100	60	10	50	114.7±1.262	0.31±0.003	0.76±0.013
24	200	100	60	10	100	112.1±0.561	0.37±0.002	0.76±0.012
25	200	100	120	5	100	116.4±1.513	0.21±0.004	0.81±0.016
26	200	100	60	15	75	130.4±1.956	0.33±0.002	0.75±0.008
27	200	100	120	10	75	101.9±0.713	0.23±0.002	0.83±0.012
28	200	100	120	10	75	117.2±0.938	0.26±0.004	0.86±0.009
29	200	50	180	10	75	314.3±1.886	0.51±0.004	0.8±0.016
30	200	150	120	10	100	144.2±2.451	0.2±0.002	0.85±0.009
31	200	100	120	10	75	117.7±1.883	0.26±0.004	0.84±0.015
32	300	100	60	10	75	159.3±1.274	0.3±0.004	0.9±0.009
33	200	100	120	15	50	170.8±3.074	0.27±0.004	0.85±0.017
34	100	100	120	15	75	191.5±1.724	0.07±0.001	0.81±0.015
35	200	50	120	5	75	199.3±0.997	0.28±0.003	0.77±0.009
36	300	100	120	15	75	289.8±5.796	0.37±0.004	0.92±0.010
37	300	100	180	10	75	206.4±2.270	0.11±0.002	0.95±0.019
38	200	100	60	5	75	120.8±2.054	0.47±0.008	0.75±0.010
39	300	100	120	5	75	174±2.436	0.07±0.001	0.91±0.013
40	300	150	120	10	75	110.8±2.216	0.24±0.003	0.79±0.012
41	200	150	120	10	50	180±0.900	0.28±0.004	0.89±0.013
42	200	100	120	5	50	119.2±1.550	0.35±0.003	0.82±0.015
43	300	50	120	10	75	120±2.400	0.2±0.003	0.84±0.017
44	200	100	180	15	75	278.1±3.893	0.52±0.010	0.91±0.009
45	200	150	120	5	75	178.5±2.856	0.25±0.004	0.86±0.008
	_50	100	120		. 5			2.2320.000

nta presented as mean± SD, n=3

Cultures were maintained at 37°C in a humidified incubator with a 5% CO<sub>2</sub> and 95% air atmosphere.

*Isolation of peripheral blood mononuclear cells:* 

Five mL of peripheral blood was collected from a healthy human donor via venipuncture using a disposable syringe into a tube containing ethylenediaminetetraacetic acid (EDTA) as an anticoagulant. The collected blood was diluted in a 1:1 ratio with phosphate-buffered saline (PBS) and mixed gently. Subsequently, 4 mL of Ficoll (lymphocyte separation medium, with a density of 1.077 g/mL) was added as a density gradient medium. The mixture was then centrifuged at 2000 rpm for 30 minutes at 4°C. After centrifugation, the mononuclear cell layer at the interface between the plasma and Ficoll was carefully collected using a Pasteur pipette. The isolated cells were washed

three times with 5 mL of PBS, each wash followed by centrifugation at 1500 rpm for 10 minutes. After the final wash, the supernatant was discarded, and the cell pellet was resuspended in RPMI-1640 culture medium supplemented with 10% fetal bovine serum (FBS).

#### The MTT assay

Cells are seeded in 96-well plates at an appropriate density ( $5\times10^3$  cells per well) and treated with the desired compounds. After the incubation period of 24 hours, 20  $\mu$ L of MTT solution (5 mg/mL in PBS) is added to each well, followed by incubation at 37°C for 4 hours to allow formazan crystal formation. the plate is then centrifuged at 1500–2000 rpm for 5 minutes to pellet the cells. The supernatant is carefully removed without disturbing the pellet.

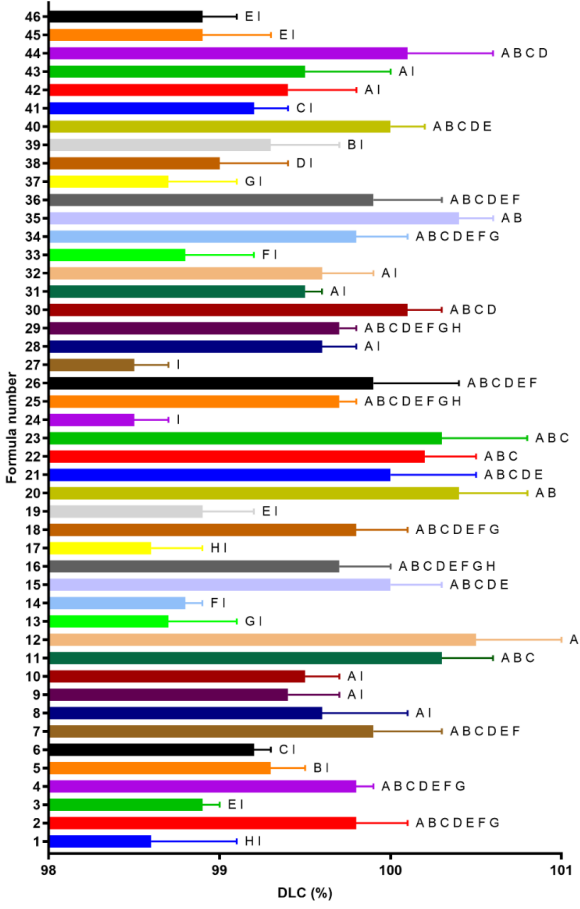


Fig. 2. Assessment of the DLC of various formulations showing the statistical analysis. Bars with similar letters indicate no significant differences. One-way ANOVA with post hoc Holm-Šídákvs multiple comparisons test was used.

Subsequently,150 µL of DMSO was added to each well to solubilize the formazan crystals, and the contents were mixed gently by pipetting or shaking. Finally, the absorbance is measured at 570 nm using a microplate reader.

MTT Assay Calculation Formulas (Eqs. 4-6)

#### Statistical analysis

Statistical analyses were performed using GraphPad Prism 10.5. Experimental data are presented as mean ± standard deviation. For the solubility study comparison, the Brown-Forsythe ANOVA test with post hoc Dunnett's T3 multiple comparisons was used to analyze differences in solubility between groups for non-parametric variables. For differences between groups in particle size, PDI, drug contents, and EE, a one-

way ANOVA with post hoc Holm-Šídák>s multiple comparisons test was employed, since the data followed a normal distribution. The level of significance was <0.05.

#### **RESULTS AND DISCUSSION**

Determination of the  $\lambda_{\max}$  in various solvents

The λmax in various solvents was determined: in distilled water, it was 327 nm (Fig. S1A); in 0.1 N HCl solution, it was 329.5 nm (Fig. S1B); in DMF, it was 324 nm (Fig. S1C); in phosphate buffer pH 6.8, it was 324 nm (Fig. S1D); in phosphate buffer saline pH 7.4, it was 326 nm (Fig. S1E); in Triton-X100 (1%) and phosphate buffer pH 6.8, it was 324 nm (Fig. S1F); in Triton-X100 (1%) and phosphate buffer saline pH 7.4, it was 325 nm (Fig. S1G); and in Triton-X100 (0.5%) and distilled water, it was 325 nm (Fig. S1H). Details are illustrated in

$$PS (nm) = 485 - 1.82 \, Span \, 60 \, + \, 0.44 \, Tween \, 60 \, + \, 0.29 \, Cholestrol \, - \, 32.2 \, SDC \, - \, 3.26 \, Soluplus \\ + \, 0.00317 \, Span \, 60^2 \, + \, 0.00940 \, Tween \, 60^2 \, + \, 0.00882 \, Cholestrol^2 \, + \, 1.900 \, SDC^2 \\ + \, 0.0466 \, Soluplus^2 \, + \, 0.00449 \, (Span \, 60 * \, Tween \, 60) \, + \, 0.00155 \, (Span \, 60 * \, Cholestrol) \\ + \, 0.0499 \, (Span \, 60 * \, SDC) \, - \, 0.0039 \, (Span \, 60 * \, Soluplus) \\ - \, 0.01300 \, (Tween \, 60 * \, Cholestrol) \, - \, 0.111 \, (Tween \, 60 * \, SDC) \\ - \, 0.0162 \, (Tween \, 60 * \, Soluplus) \, + \, 0.0109 \, (Cholestrol * \, SDC) \, - \, 0.0102 \, (Cholestrol * \, Soluplus) \\ + \, Soluplus) \, - \, 0.032 \, (SDC * \, Soluplus)$$

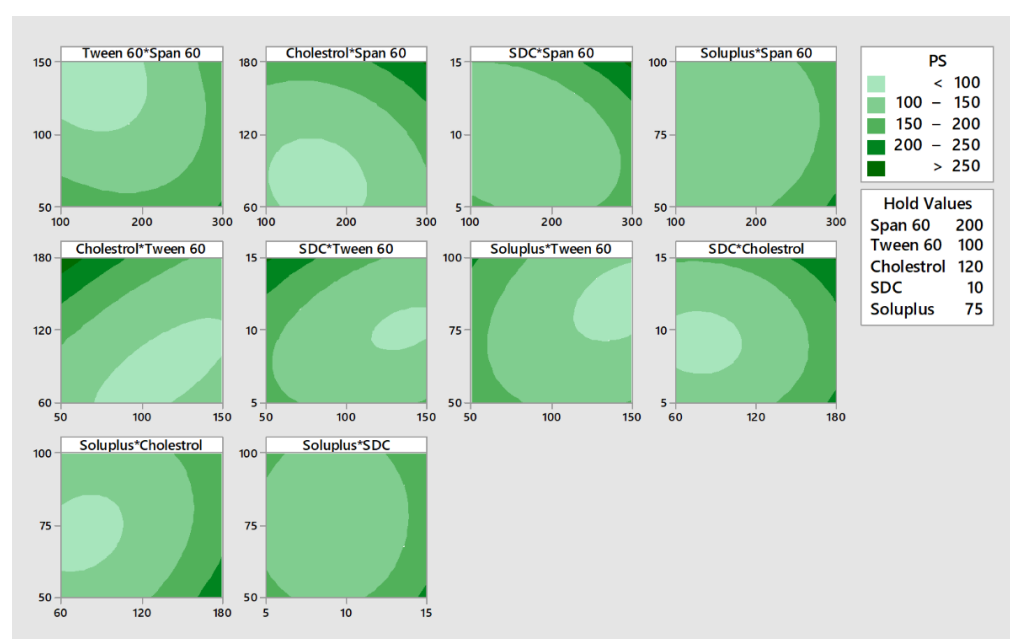


Fig. 3. Contour plot of the effect of Span 60, Tween 60, cholesterol, SDC, and soluplus on particle diameter.

the supplementary file S1 (Fig. S1).

Calibration curve of the UV spectrophotometry in various solvents

Details are illustrated in supplementary file S2, where all the coefficients of determination (R2) are  $\geq$ 0.99.

# Solubility study

Dasatinib exhibits variable solubility that can be classified into three groups: highly soluble in 0.1 N HCl, which is statistically significant compared to other solvents. It has lower solubility in both 1% Triton X-100 with PBS at pH 6.8 and 7.4 compared to 0.1 N HCl, but higher than PBS at pH 6.8 and 7.4 and in distilled water, as shown in Fig. 1.

# Optimization of dasatinib-loaded bilosomes formulation

In the current study, optimization was carried out using the Box-Behnken design (BBD), with a total of 46 formulas examined based on five factors (35) at three levels (see Table 2). Table 3 illustrates the results of each formula in terms of response parameters (PS, EE, and PDI), in which PS ranged from 89.8±1.527 to 314.3±1.886 nm (see Fig. S3), PDI ranged from 0.05±0.001 to 0.515±0.010% (Fig. S4), and EE ranged from 0.73±0.004 to

0.95±0.019% (Fig. S5).

# Drug content

All formulas show excellent drug content ranging from 98.5±0.20 to 100±0.50%, as seen in Fig. 2.

#### Effect on particle diameter (Y1)

By holding the effect of three parameters, the change in effect of the other two parameters can be examined to determine their effect on PS. There was an inverse relationship between Span 60 and Tween 60, in which high Tween 60 and low Span 60 were associated with low PS. Direct relationship between the following pairs: 1) cholesterol and Span 60, 2) SDS and Span 60, 3) SDS and cholesterol. Inverse correlation between the following pairs: 1) Tween 60 and Span 60, 2) cholesterol and Tween 60, 3) SDS and Tween 60. Soluplus did not have any association with the other four parameters, as illustrated in Figs. 3 and S7.

The overall  $R^2$  of the model was 63.82%. Cholesterol had the highest impact (p-value = 0.001), followed by Tween 60 (p-value = 0.014) and Span 60 (p-value = 0.030). In contrast, the SDS (p-value = 0.174) and soluplus (p-value = 0.676) had a significant impact on PS. The final model is illustrated in the Eq. 7.

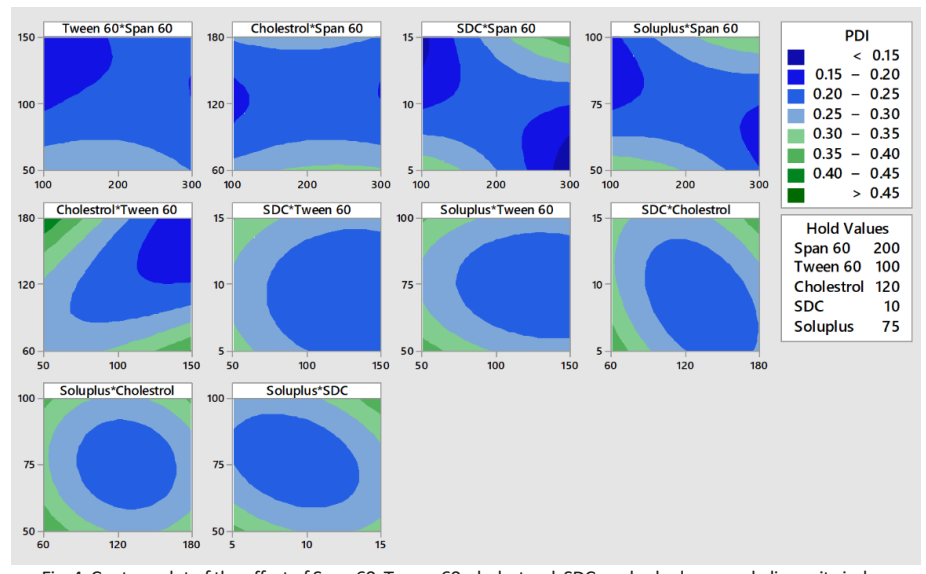


Fig. 4. Contour plot of the effect of Span 60, Tween 60, cholesterol, SDC, and soluplus on polydispersity index.

# Effect on polydispersity index (Y2)

By holding the effect of three parameters, the change in effect of the other two parameters can be examined to determine their effect on PDI. There was an inverse relationship between Span 60 and Tween 60, in which high Tween 60 and

low Span 60 were associated with low PDI. Direct relationship between cholesterol and Tween 60. Inverse correlation between SDS and cholesterol. The rest of the parameters show a variable relationship that cannot be explained by linear relationships, such as the combination of high SDS

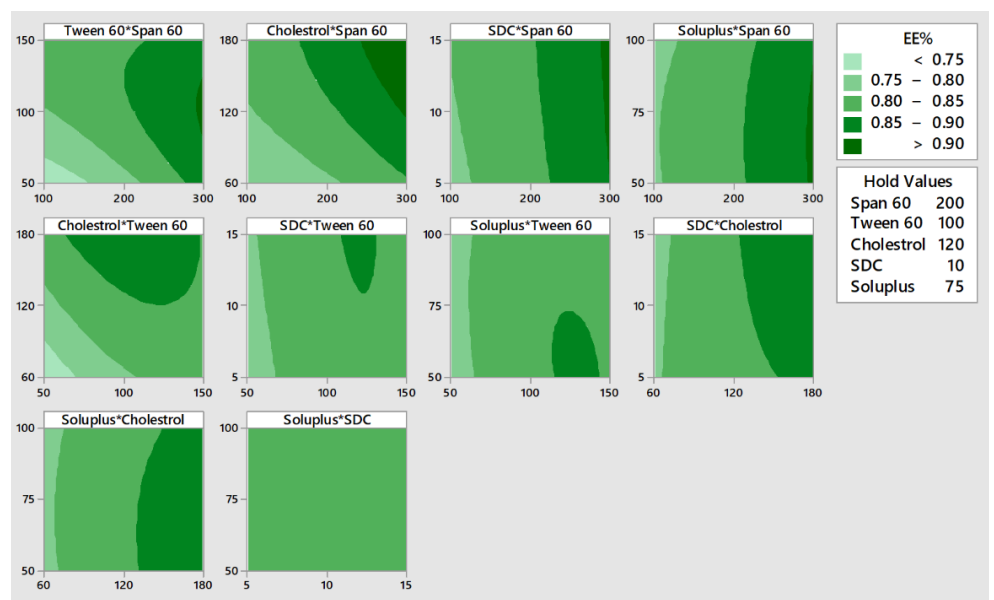


Fig. 5. Contour plot of the effect of Span 60, Tween 60, cholesterol, SDC, and soluplus on entrapment efficiency.

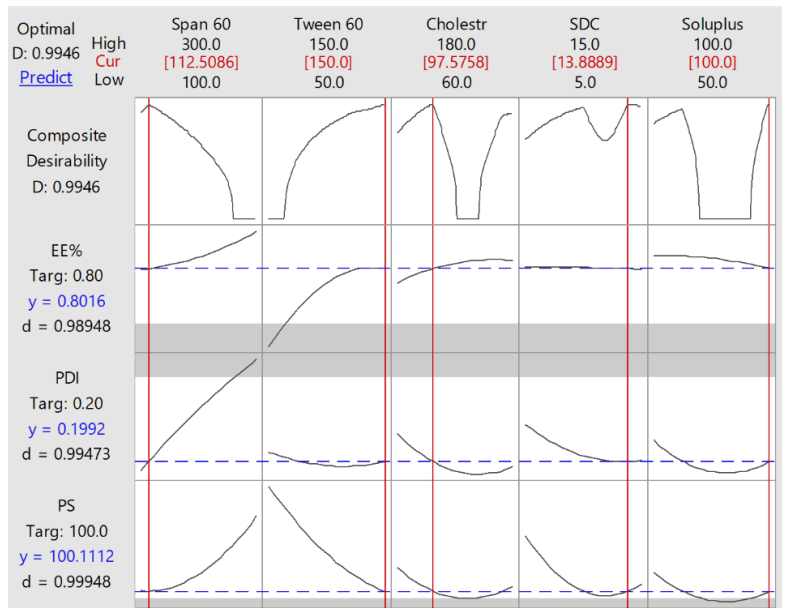


Fig. 6. The desirability value for optimized formulation.

and lower Span 60, or lower SDS and high Span 60, which resulted in low PDI, as illustrated in Figs. 4 and S8.

The overall  $R^2$  of the model was 48.01%, Tween had the highest impact on PDI (r= -0.0436,

p-value = 0.140), followed by cholesterol (p-value = 0.503), SDS (p-value = 0.605), Span 60 (p-value = 0.863), and soluplus (p-value = 0.897), all these parameters did not reach statistical significance. The final model is illustrated in the Eq. 8.

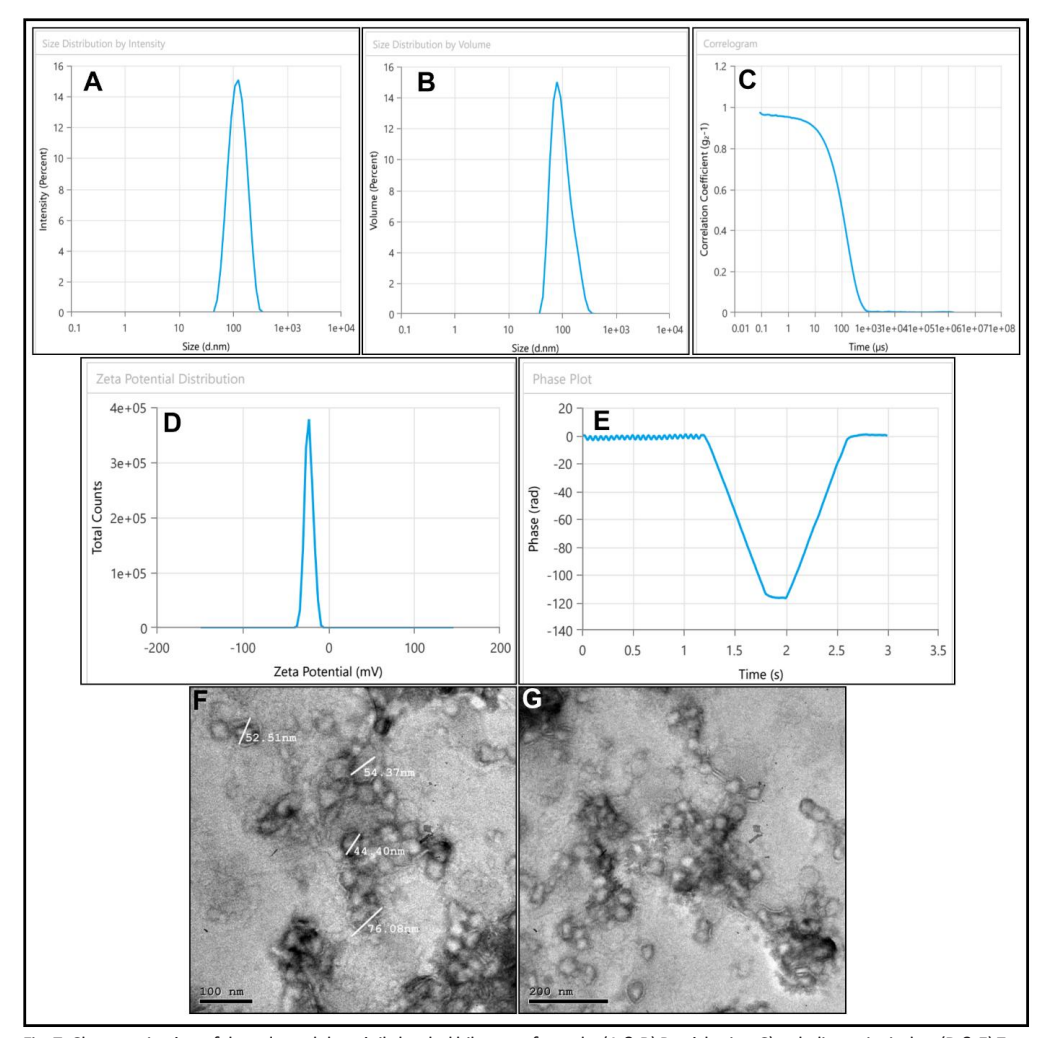


Fig. 7. Characterization of the selected dasatinib-loaded bilosome formula. (A & B) Particle size, C) polydispersity index, (D & E) Zeta potential, (F &G) TEM of the optimized bilosomal formulation containing dasatinib at two magnifications at 100 nm bar scale, and 200 nm bar scale.

Table 3. The characteristics of the predicted and actual for the dasatinib-loaded bilosome formula.

Variables —	Dasatinib-loaded bilosome		
variables —	Actual	Predicted	
Z-average (nm)	113.2 ± 0.64	100.112	
Polydispersity Index (%)	0.1094 ± 0.002	0.1992	
Zeta potential (mV)	-22.36 ± 1.21	-	
Entrapment efficiency (%)	81.02 ± 0.021	80.16	

Data presented as mean ± standard deviation (each value represents a triple)

# Effect on entrapment efficiency (Y3)

By holding the effect of three parameters, the change in effect of the other two parameters can be examined to determine their effect on EE. There was a direct relationship between Span 60 and Tween 60, in which high Tween 60 and high Span 60 were associated with high EE. Direct relationship between the following pairs: 1) Tween 60 and Span 60, 2) cholesterol and Span 60, 3) cholesterol and Tween 60. Soluplus and SDS did not have any association with the other three parameters, as illustrated in Figs. 5 and S8.

The overall  $R^2$  of the model was 75.43%. Span 60 had the highest impact on EE (p-value < 0.001), followed by cholesterol (p-value < 0.001) and Tween 60 (p-value = 0.004). In contrast, the SDS (p-value = 0.573) and soluplus (p-value = 0.669) did not reach statistical significance. The final model is illustrated in the Eq. 9.

#### Selection of the Optimized Formula

The optimized formula was chosen by the numerical optimization of Minitab\* 17.1.0 \$\( \text{software} \) based on the desirability factor's proximity to 1. The predicted cholesterol (x1= 112.5 mg), Tween 60 (x2= 150 mg), Span 60 (x3= 97.6 mg), SDS (x4= 13.9 mg), and Soluplus (x5= 100 mg) were acquired, and this was selected as the optimized \$\( \text{formula} \) with a desirability of 0.9946, as seen in Fig. 6.

Characterization of dasatinib-loaded bilosomes formulation

Particle size and PDI

The Z-average, or the average particle size, was

measured to be  $113.2 \pm 0.64$  nm, while the model predicted it to be 100.112 nm. The actual value is slightly higher than the predicted value, indicating a minor deviation from the model's prediction, as illustrated in Figs. 7A and 7B and Table 3.

The PDI measures the uniformity of particle sizes within the formulation. The actual PDI is  $0.1094 \pm 0.002\%$ , which is lower than the predicted value of 0.1992%. A lower PDI indicates a more uniform particle size distribution, suggesting that the actual formulation is more uniform than predicted, as illustrated in Fig. 7C and Table 3.

#### Zeta potential

The zeta potential measures the surface charge of the particles, which affects their stability. The actual zeta potential is -22.36  $\pm$  1.21mV. A negative zeta potential indicates that the particles are likely to repel each other, contributing to the stability of the formulation, as illustrated in Figs. 7D and 7E and Table 3.

# Entrapment efficiency

Entrapment efficiency refers to the percentage of dasatinib successfully encapsulated within the bilosomes. The actual entrapment efficiency is  $81.02\pm0.021\%$ , which is very close to the predicted value of 80.16%, indicating that the model accurately predicted this parameter, as illustrated in Table 3.

The optimized formula shows uniform, spherical vesicle morphology and confirms successful bilayer self-assembly. Additionally, the images show unilamellar vesicles from multilamellar structures, as seen in Figs. 7F and 7G.

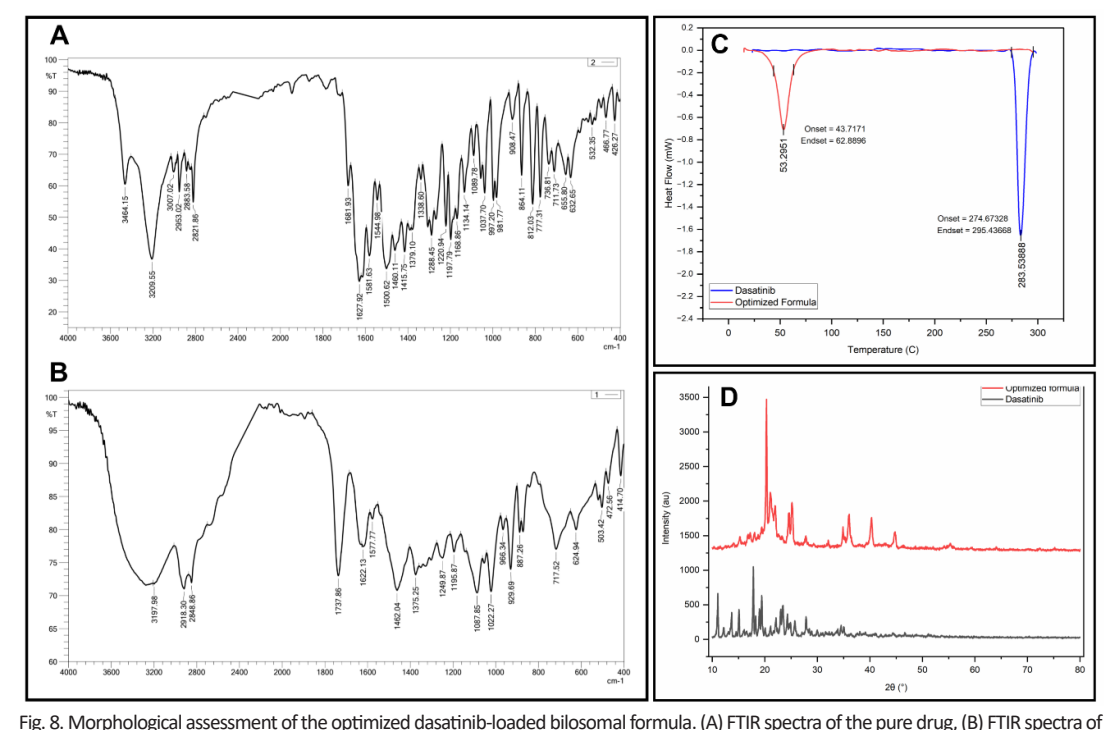
\* SDC) - 0.000002 (Cholestrol \* Soluplus) + 0.000013 (SDC \* Soluplus)

#### FTIR studies

The infrared absorption spectrum of the pure dasatinib drug displays several diagnostically significant vibrational bands that are consistent with its known functional groups. N-H Stretching: A prominent absorption feature appears around 3197 to 3200 cm<sup>-1</sup>, which can be assigned to the stretching vibrations of a secondary amine (N–H), commonly present in heterocyclic pharmacophores. C-H Stretching Vibrations: Additionally, well-defined bands near 2918 cm<sup>-1</sup> correspond to aliphatic C-H stretching modes, indicating the presence of saturated hydrocarbon chains or methylene groups within the molecule. Aromatic Ring Stretching: An intense band located between 1640 and 1622 cm<sup>-1</sup> is ascribed to the stretching vibrations of either C=N or C=C bonds, likely originating from the quinazoline core or other aromatic systems of the molecule. Further support for the aromatic nature of Dazatinib comes from bands appearing between 1577 and 1581 cm<sup>-1</sup>, attributed to stretching within conjugated aromatic rings. The spectral data also show a welldefined peak at approximately 1462 cm<sup>-1</sup>, which corresponds to bending motions of methylene

(CH<sub>2</sub>) groups, suggesting structural retention of side chains. C–N and C–O Stretching: A vibration at 1375 cm<sup>-1</sup> is indicative of symmetric stretching involving either C–N bonds or the sulfonyl (SO<sub>2</sub>) group, both common in kinase inhibitors like Dazatinib. Another notable absorption appears at 1249 cm<sup>-1</sup>, assignable to either C–F or C–O stretching, further supported by bands in the 1195 to 1160 cm<sup>-1</sup> range that are characteristic of sulfone or aryl-fluoride functional groups, as seen in Figs. 8A and 8B.

Out-of-Plane C–H Bending and Halogen Modes: Lastly, the region between 1022 and 1037 cm<sup>-1</sup> exhibits aromatic C–H deformation modes, while bending vibrations associated with aromatic substitution patterns can be observed near 870 to 750 cm<sup>-1</sup>. The FTIR spectrum of the lyophilized dasatinib-loaded bilosomal formulation revealed several retained peaks, each corresponding to characteristic functional groups within the dasatinib molecule or its associated excipients. A broad absorption band centered at 3298 cm<sup>-1</sup> is attributed to the N–H stretching vibration of secondary amines, indicating the preservation of the amine functionality within the heterocyclic



the lyophilized dasatinib-loaded bilosomal, (C) DSC thermogram of pure Dasatinib (blue line) and lyophilized dasatinib-loaded bilosomal (red line), (D) The XRD diffractogram of the pure and optimized dasatinib. (The image drawn using OriginLab 2024).

framework of dasatinib. This peak may also overlap with O–H stretching vibrations from hydroxyl-containing excipients such as mannitol or cholesterol, and its broad nature suggests the involvement of hydrogen bonding. An absorption band observed at 1737 cm<sup>-1</sup> corresponds to carbonyl (C=O) stretching vibrations, likely arising from residual ester or amide linkages present either in the drug structure or the formulation excipients (e.g., surfactants). The presence of this band supports the structural retention of carbonyl-containing functionalities.

A prominent peak at 1622 cm<sup>-1</sup> is associated with the stretching of conjugated C=C or C=N bonds, indicating the presence of aromatic or heteroaromatic systems such as the quinazoline core of dasatinib. This peak serves as strong evidence for the preservation of the aromatic framework of the drug. The band at 1375 cm<sup>-1</sup> is assigned to the symmetric stretching vibration of sulfonyl (SO<sub>2</sub>) groups or alternatively to C-N stretching modes, both of which are present in the molecular structure of dasatinib. The retention of this peak indicates that the sulfonamide moiety, a critical pharmacophoric component, remains chemically intact. The absorption peak at 1249 cm<sup>-1</sup> is suggestive of C-O, C-F, or S=O stretching, reflecting the possible presence of aryl fluoride groups, ether linkages, or sulfonyl functionalities, all of which are relevant to dasatinib and its

formulation matrix. This confirms that no cleavage or major transformation of these moieties has occurred during processing. Finally, the band at 1022 cm<sup>-1</sup> is attributed to aromatic C–H deformation or to C–N/C–O stretching vibrations, supporting the presence of intact aromatic substitution patterns and heteroatom-linked side chains, as seen in Figs. 8A and 8B.

#### DSC studies

The DSC thermogram of pure dazatinib (Fig. 8C) exhibited a sharp endothermic peak at 283.53888 °C, with an onset at 274.67328 °C and an endset at 295.43668 °C. This thermal event corresponds to the melting point of crystalline dazatinib, confirming its highly ordered crystalline structure in the pure form, which is consistent with previous studies [11, 46, 47]. In contrast, the DSC thermogram of the lyophilized dasatinib-loaded bilosomal (Fig. 8C), composed of dasatinib and bilosome components including Span 60, Tween 60, cholesterol, and mannitol, showed a broad endothermic peak centered at 53.2951 °C, with an onset at 43.7171 °C and an endset at 62.8896 °C, which is consistent with the melting transition of Span 60. No thermal event was observed near the dasatinib melting range.

# XRD studies and crystallinity index

The XRD diffractogram of pure dazatinib

Table 4. Assessment of drug release kinetics for various formulas.

Variables —	Dasatinib-loaded bilosome			
variables —	Actual	Predicted		
Z-average (nm)	113.2 ± 0.64	100.112		
Polydispersity Index (%)	0.1094 ± 0.002	0.1992		
Zeta potential (mV)	-22.36 ± 1.21	-		
Entrapment efficiency (%)	81.02 ± 0.021	80.16		

Data presented as mean ± standard deviation (each value represents a triple)

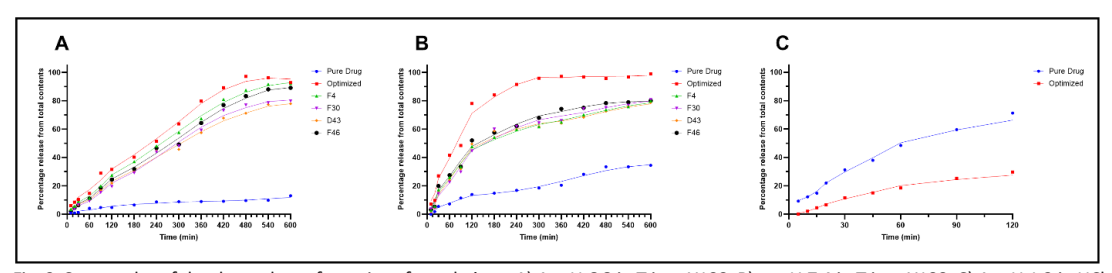


Fig. 9. Scatter plot of the drug release for various formulations. A) At pH 6.8 in Triton-X100, B) at pH 7.4 in Triton-X100, C) At pH 1.2 in HCl solution.

revealed several sharp and intense diffraction peaks, particularly in the range of  $10^{\circ}$  to  $30^{\circ}$   $2\theta$ , confirming its highly crystalline nature with CI = 71.1%. In contrast, the dazatinib-loaded bilosome formulation showed a marked reduction in peak intensity and sharpness, with some peaks either broadened or completely absent, indicating a substantial loss of crystallinity (CI% = 46.3%).

This transformation suggests that dazatinib was successfully incorporated into the bilosomal matrix in an amorphous or molecularly dispersed state, likely due to interactions with excipients such as Span 60, Tween 60, cholesterol, SDC, and Soluplus. Furthermore, mannitol, used during lyophilization, may have acted as a cryo-/lyoprotectant, contributing to the stabilization of the amorphous form and inhibiting drug recrystallization during the freeze-drying process,

as illustrated in Fig. 8D.

# In vitro drug release study

Table 4 provides an overview of different mathematical models used to describe drug release kinetics and includes experimental data to evaluate how well these models fit various formulations under different conditions. The optimized formulations generally show better model fits, indicating more controlled and predictable drug release patterns. Additionally, at pH 6.8, (51.3% vs. 8.7%) of the drug was released after 240 minutes, (79.7% vs. 9.0%) after 360 minutes, and (92.75% vs. 13.0%) after 600 minutes for optimized versus pure dasatinib. At pH 7.4, (48.4% vs. 11.4%) was released after 90 minutes, (70.1% vs. 13.9%) after 120 minutes, and (98.9% vs. 34.4%) after 600 minutes for optimized versus

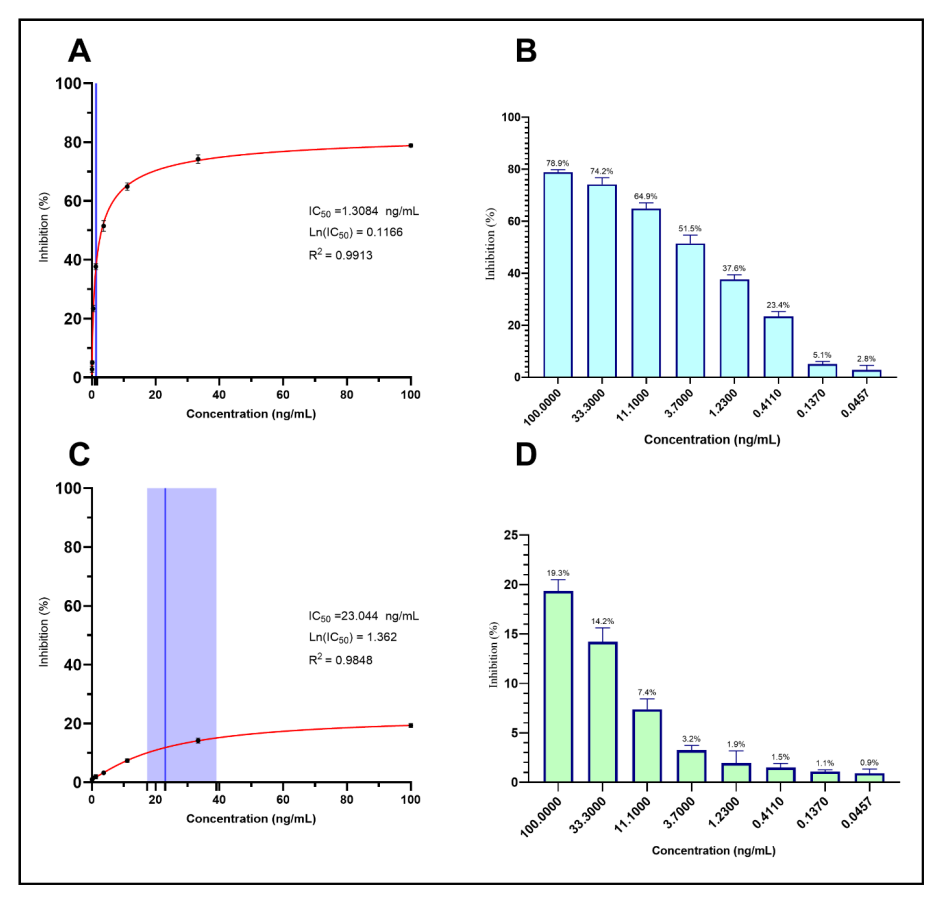


Fig. 10. The activity of optimized dasatinib-loaded bilosomes formulation against chronic myeloid leukemia cell lines and normal lymphocytes. A) The  $\rm IC_{50}$  in the K562 cell line, B) Histogram of the percentage inhibition in the K562 cell line, C) The  $\rm IC_{50}$  in normal lymphocytes, D) Histogram of the percentage inhibition in normal lymphocytes. (inhibitor vs. response-Variable slope (four parameters) was used).

pure dasatinib, as shown in Fig. 9. Based on these results, we examined the release profile of the optimized formula under acidic conditions (pH 1.2) to assess the extent of drug release. It reveals that 11.6% of the drug in the optimized formula was released after 30 minutes, 18.4% after 60 minutes, and 29.7% after 120 minutes. In contrast, for pure dasatinib, 31.2% was released after 30 minutes, 48.4% after 60 minutes, and 71.2% after 120 minutes, indicating that this formula is best taken on an empty stomach to prevent significant early drug release in the stomach.

Phosphate-buffered saline (pH 6.8) containing Triton-X100: for the pure drug, the  $R^2$  values range from 0.6310 to 0.8521, indicating varying degrees of fit for different models. While for the optimized formula, the  $R^2$  values are higher, ranging from 0.9293 to 0.9808, suggesting a better fit for the models. Meanwhile, formulations F4, F30, F43, and F46 also show high  $R^2$  values, indicating good model fits.

Phosphate-buffered saline (pH 7.4) containing Triton-X100: for the pure drug, the R² values range from 0.9202 to 0.9627. While for the optimized formula, the R² values are lower for some models, with a notable drop to 0.2954 for the zero-order model. Meanwhile, formulations F18, F27, F38, and F41 show varying degrees of fit, with some models fitting better than others.

For HCl solution (pH 1.2): for the pure drug, the  $R^2$  values range from 0.8726 to 0.9912. While for the optimized formula, the  $R^2$  values range from 0.8629 to 0.9792, indicating that the optimized formula followed first-order kinetics.

For the optimized formula, the best model for describing the drug release kinetics is the Korsmeyer-Peppas model in phosphate-buffered (pH 6.8 and 7.4) containing Triton-X100. At the same time, in HCl solution, it followed first-order kinetics. This model showed the highest correlation coefficient (R² value) of 0.9742 in phosphate-buffered (pH 6.8 and 7.4) containing Triton-X100, while in HCl solution, the R² was 0.9943. This indicates that the Korsmeyer-Peppas model provides the best fit for the drug release data under these conditions, suggesting a more controlled and predictable drug release profile.

Regarding the drug release mechanism for the optimized formula at pH 6.8, N = 0.720; at pH 7.4, N = 0.397; and at pH 1.2, N = 0.823, this indicates that at pH 7.4, the drug follows a Fickian diffusion mechanism. In contrast, at pH 6.8 and 1.2, the

drug demonstrates non-Fickian transport.

In vivo assessment of the optimized formula (MTT study)

The optimized formula demonstrates a significant inhibitory effect against chronic myeloid leukemia cell lines (K562), with an IC50 of 1.308 ng/mL, which is lower than that observed in normal lymphocytes, with an IC50 of 23.044 ng/mL. This confirms the anticancer activity of the optimized formula and its relative safety for normal human lymphocytes, as shown in Fig. 10.

Bilosomes are bile salt-stabilized nanovesicles (essentially liposomes or niosomes incorporating bile acids into their structure). They have emerged as a promising strategy to overcome oral delivery challenges, especially for drugs like dasatinib that are poorly water-soluble and unstable across GI conditions [49]. Dasatinib is a potent tyrosine kinase inhibitor but belongs to Biopharmaceutics Class II (BCS II), meaning it has very low aqueous solubility and decent permeability [50, 51]. This poor solubility severely limits its oral bioavailability (reported absolute bioavailability is only ~14-34%) [52]. Moreover, dasatinib's solubility is highly pHdependent – it dissolves in acidic gastric fluid. Still, it precipitates in near-neutral intestinal pH (solubility drops from ~18 mg/mL at pH ~2.6 to virtually <0.001 mg/mL at pH ~7) [7]. This is consistent with the study observations that dasatinib has its highest solubility in 0.1 N HCl (50.1 mg/mL), and its solubility drastically decreases in PBS solution at pH 6.8 (0.0095 mg/mL) and 7.4 (0.0111 mg/ mL). Even after adding cosolvent, it remains low (0.21 and 0.25 mg/mL). As a result, when the drug passes from the stomach into the higher pH intestine, a significant fraction may precipitate out, reducing the amount available for absorption. Additionally, dasatinib undergoes extensive firstpass metabolism, further curtailing the fraction reaching systemic circulation [7, 53-55]. These factors motivate the need for a specialized oral formulation that can enhance solubility, protect the drug through varying GI pH, and potentially bypass some first-pass loss.

Based on these rationales, the formulation strategy for dasatinib-loaded bilosomes involved creating stable nanovesicles composed of a nonionic surfactant, cholesterol, and a bile salt, with dasatinib encapsulated in their lipid bilayer. In practice, a reverse-phase evaporation technique was employed — a classic method for vesicle

preparation known to yield high encapsulation efficiency. This entailed dissolving the lipid/surfactant (e.g., Span 60 or a phospholipid), cholesterol, and dasatinib in an organic solvent, forming a thin film by solvent evaporation, and then hydrating the film with an aqueous phase containing bile salt (sodium deoxycholate) and Soluplus (dual role as a solubilizer and stabilizer in solid dispersions, preventing drug recrystallization and enhancing dissolution rates [56]), under agitation to self-assemble bilosomes. The inclusion of cholesterol helps to rigidify and stabilize the bilosomal membrane, preventing leakage [57], whereas the bile salt imparts elasticity and a negative surface charge [58].

The current study findings highlight the effectiveness of the optimization model in predicting the characteristics of the dasatinibloaded bilosome formula. While there are minor deviations between the predicted and actual values, the overall predictions are quite accurate, particularly for the entrapment efficiency. The lower PDI and the negative zeta potential suggest that the actual formulation is stable and has a uniform particle size distribution.

Formulation optimization was key to achieving desirable properties. A design-of-experiments approach (Box-Behnken design) was used to optimize factors like the surfactant-to-cholesterol ratio and the bile salt concentration [59]. These factors significantly influence vesicle size, drug entrapment, and release. For instance, too high a bile salt fraction can destabilize the bilayer and cause drug leakage, while too little may not confer enough stability or permeability enhancement [60, 61]. The chosen optimized formulation balanced these components to produce nanosized bilosomes with maximal drug loading. In summary, the formulation strategy centered on encapsulating dasatinib within bile-stabilized nanovesicles that are robust enough for oral delivery and tuned for efficient drug loading and release in the intestine.

After formulation, the dasatinib-loaded bilosomes were extensively characterized to ensure they met the desired specifications for oral delivery. Key physicochemical properties measured include particle size (and size distribution), surface charge (zeta potential), drug encapsulation efficiency, morphology, and the physical state of the drug inside the carriers.

The bilosomes had an average diameter on the order of only a few hundred nanometers

 $(113.2 \pm 0.64 \text{ nm for the optimized formulation}).$ This nanoscale size was confirmed by dynamic light scattering (ranging from 44.4 to 76.08 nm), which also indicated a relatively low PDI (0.1094 ± 0.002%), signifying a homogeneous vesicle population with a narrow size distribution. Such small, uniform particles are ideal for oral absorption, as they can penetrate mucus layers and be taken up by intestinal cells more readily than larger or polydisperse particles. Literature reports of similar bilosomal systems likewise show mean diameters in the 100-300 nm range, aligning with these results. The small size and uniformity suggest the formulation process was well-controlled and reliable for reproducible nanoparticle production [59, 62].

Several explanations for the discrepancy in particle between the measures. DLS measures the hydrodynamic diameter of particles in suspension, which includes the solid core plus any surfacebound solvent molecules, surfactant layers, and diffuse electrical double layer. This typically yields larger size values than direct imaging [63, 64]. TEM, by contrast, measures the projected physical diameter of dried or vitrified particles under high vacuum. The absence of the hydration shell and possible particle shrinkage during sample preparation often result in smaller measured sizes. DLS also reports an intensityweighted average, which is disproportionately influenced by even a small fraction of larger aggregates, whereas TEM provides numberweighted size distributions from the imaged population. Furthermore, sample preparation differences (e.g., drying, staining, vacuum exposure) in TEM can cause vesicle collapse or deformation, further reducing apparent size compared to the hydrated state measured by DLS [64, 65].

The zeta potential of dasatinib-loaded bilosomes was found to be moderately negative (approximately  $-22.36 \pm 1.21$  mV). The negative charge comes from the presence of deprotonated bile salts (e.g., deoxycholate) embedded in the bilayer [66]. A sufficiently high magnitude zeta potential is beneficial for colloidal stability because it generates electrostatic repulsion between vesicles, preventing aggregation [67]. The observed negative zeta potential indicates the bilosomal suspension is electrostatically stabilized, which is consistent with other bile-containing vesicles in the literature that report zeta potentials in the -20 to -50 mV range. This stability is

crucial for maintaining the formulation's integrity both in storage and upon dilution in biological fluids. Additionally, surface charge can influence interaction with biological membranes; the negatively charged bilosomes may have reduced nonspecific adhesion to the negatively charged mucosal lining, potentially prolonging their transit and making uptake more targeted [59].

The formulation achieved a high encapsulation efficiency of 81.02 ± 0.021%, meaning the majority of the dasatinib added during preparation was successfully entrapped within the bilosomal vesicles rather than lost in the external phase. Such a high EE% is indicative of the strong affinity of hydrophobic dasatinib for the lipid/surfactant bilayer. Dasatinib's poor water solubility actually becomes advantageous in this context, as it tends to partition into the hydrophobic core of the bilayer during formulation [55]. Similar bile-based nanoformulations often report high EE (for instance, >90% of a hydrophobic drug encapsulated). The optimized composition (appropriate surfactant, cholesterol, and bile salt ratio) likely minimized drug leakage by creating a stable yet accommodating bilayer environment. A high EE is important for ensuring that a given dose of the nanoparticle formulation delivers a sufficient amount of drug. In practical terms, ~81% EE implies that if 100 mg of dasatinib were used in preparing bilosomes, about 81 mg is encapsulated in the vesicles. This efficiency is especially beneficial for potent, expensive drugs like dasatinib, as it maximizes payload without excessive waste [62].

Transmission electron microscopy (TEM) imaging revealed that the dasatinib-loaded bilosomes are spherical vesicles with smooth surfaces, and no significant aggregation was observed among particles (corroborating the DLS findings of low PDI). The vesicles appeared as distinct, well-formed spherical structures, which is characteristic of successful bilosome formation [62]. The absence of visible crystals or phase separation in the micrographs suggests that dasatinib is not present as large crystalline domains but is rather uniformly distributed within the vesicle membranes. Additional physicochemical analyses were performed to assess the drug's physical state and any drug-excipient interactions: Differential scanning calorimetry (DSC) thermograms of the lyophilized bilosomes did not show the sharp melting endotherm of crystalline dasatinib,

implying the drug is likely in an amorphous or molecularly dissolved state within the lipid matrix. This amorphization can contribute to the improved dissolution behavior of the drug. In the bilosomal formulation containing dasatinib, the characteristic sharp melting peak of dasatinib at ~284 °C was absent. This disappearance indicates that dasatinib no longer exists in its crystalline form and is likely to be amorphous or molecularly dispersed within the bilosomal matrix [11, 46, 47].

The FTIR spectrum of the lyophilized dasatinibloaded bilosomal formulation revealed the presence of several characteristic vibrational bands consistent with the intact chemical structure of dasatinib. These retained peaks are indicative of preserved functional groups and the absence of significant degradation or structural modification during the formulation and lyophilization processes. A broad absorption band was observed at 3298 cm<sup>-1</sup>, which is attributed to the N-H stretching vibration of the secondary amine group inherent in dasatinib's heterocyclic moiety. The broadness of this peak may be influenced by overlapping O-H stretching vibrations from hydroxyl-containing excipients such as mannitol or cholesterol, and suggests potential hydrogen bonding interactions within the formulation matrix. A well-defined absorption band at 1737 cm<sup>-1</sup> corresponds to the C=O stretching vibration, likely originating from residual amide or ester linkages present either within the drug molecule or among the formulation excipients (e.g., surfactants such as Span 60 or Tween 60). The persistence of this peak suggests the retention of carbonyl-containing functionalities. The strong band at 1622 cm<sup>-1</sup> is assigned to C=N and/or aromatic C=C stretching vibrations, confirming the preservation of the quinazoline core and other aromatic systems in the dasatinib molecule. A peak at 1375 cm<sup>-1</sup> is ascribed to symmetric S=O stretching of the sulfonamide moiety, or to C-N stretching, both of which are integral to dasatinib's pharmacophoric structure. The retention of this band affirms the chemical integrity of the sulfonyl functional group. The absorption band at 1249 cm<sup>-1</sup> can be attributed to overlapping C-O, C-F, or S=O stretching vibrations, reflecting the presence of aryl fluoride substituents, ether linkages, or sulfonyl groups. The maintenance of this region supports the preservation of dasatinib's side chain functionalities. Finally, a peak at 1022 cm<sup>-1</sup> was retained, which corresponds to C-N

and C-O stretching, as well as aromatic C-H deformation vibrations. This band supports the continued presence of heteroatom-linked aromatic structures, such as substituted phenyl or heteroaryl moieties. The retention of the aforementioned FTIR peaks—namely those at 3298, 1737, 1622, 1375, 1249, and 1022 cm<sup>-1</sup> demonstrates the structural stability of dasatinib within the bilosomal system. The absence of major shifts or loss of key functional group bands indicates that no significant chemical degradation or covalent modification occurred during bilosome encapsulation and lyophilization. These results provide strong spectroscopic evidence supporting the compatibility and stability of dasatinib in the bilosomal carrier. FTIR spectroscopy also indicated no chemical incompatibilities; the characteristic peaks of dasatinib were still present in the bilosome spectrum. This indicates no interactions hydrogen bonding between dasatinib and the bilosomal constituents. Overall, the characterization data confirm that the formulated bilosomes encapsulate dasatinib efficiently in a stable, nanosized vesicular form, setting the stage for improved drug delivery performance.

The XRD diffractogram of pure dazatinib displayed multiple sharp reflections between 10° and 30°, indicating a highly ordered crystalline structure with a crystallinity index (CI) of 71.1%. Conversely, the dazatinib-loaded bilosomes exhibited diminished and broadened peaks, with some peaks partially disappearing, resulting in a significantly lower CI of 46.3%. This suggests a shift toward a less ordered state, likely due to partial amorphization or molecular dispersion of the drug within the vesicular matrix, rather than simply peak masking, as evidenced by both the reduction in intensity and peak broadening. These XRD patterns are commonly associated with amorphous or mesomorphic drug forms in lipid or surfactant-based systems [68-70].

Lyophilization with mannitol likely helped preserve the disordered state after drying. As a cryo-/lyoprotectant and bulking agent, mannitol can prevent ice- and dehydration-induced vesicle fusion, maintain particle integrity, and decrease mobility that leads to drug recrystallization during freezing and primary drying. While mannitol's crystallization behavior must be controlled through process conditions and formulation, its protective effect on lipid/surfactant vesicles is well-established, and the lack of restored

drug crystallinity indicates effective stabilization [71, 72]. Partial amorphization and molecular dispersion generally increase configurational entropy and free energy. This can enhance the apparent solubility and dissolution rate, which are crucial for the exposure of poorly water-soluble active compounds—assuming the amorphous state remains stable against recrystallization during storage and dispersion [68, 69]. The XRD results, therefore, support the intended bilosomal design: to incorporate dazatinib within a soft-matter matrix that reduces crystallinity and improves the drug's ability to dissolve.

The combination of XRD peak attenuation and broadening with a CI decrease to 46.3%, the disappearance of dasatinib's melting endotherm in DSC, along with FTIR bands that are still present but widened—indicating hydrogen-bonding interactions—together with TEM evidence of bilayer vesicles, strongly suggests that dasatinib exists mainly in an amorphous or molecularly dispersed form within the bilosomal matrix. This state is maintained through interactions between the drug, surfactant, or polymer, and is further stabilized by lyoprotection.

The in vitro drug release study provides valuable insights into the release kinetics of various formulations under different conditions. The study employs several mathematical models to describe the drug release kinetics, and the results indicate that the optimized formulations generally exhibit better model fits, suggesting more controlled and predictable drug release profiles.

The study identifies the Korsmeyer-Peppas model as the best model for describing the drug release kinetics of the optimized formula. This model showed the highest correlation coefficient (R<sup>2</sup> value) of 0.9742 in phosphate-buffered saline (pH 6.8 and 7.4) containing Triton-X100. This indicates that the Korsmeyer-Peppas model provides the best fit for the drug release data under these conditions, suggesting a more controlled and predictable drug release profile. The mechanism of drug release for the optimized formula varies with pH. At pH 6.8, the release exponent (N) is 0.720, indicating non-Fickian transport. At pH 7.4, the release exponent (N) is 0.397, suggesting a Fickian diffusion mechanism. This variation in the release mechanism highlights the importance of the formulation and environmental conditions in determining the drug release profile.

Previous studies have highlighted the challenges

of delivering dasatinib in the gastrointestinal (GI) environment due to the destabilizing effects of bile salts on conventional lipid vesicles, which can lead to premature drug release. Building on these insights, the current study demonstrates that bilosomes, which inherently contain bile salts in their bilayer, offer a significant advantage by resisting the solubilizing action of additional bile in the gut [62]. This property allows bilosomes to survive the harsh GI conditions without disintegrating, effectively protecting the encapsulated dasatinib from degradation or precipitation as it transits from the stomach to the intestine [7]. The efficacy of this approach is reflected in our formulation's high encapsulation efficiency (81.02 ± 0.021%), small particle size (113.2  $\pm$  0.64 nm), and negative charge (-22.36  $\pm$ 1.21 mV), confirming the potential of bilosomes to enhance dasatinib delivery.

Enhanced solubility and dissolution are another advantage; encapsulating dasatinib in the lipidic bilayer of bilosomes keeps the drug in a dissolved or molecularly dispersed form. This nanocarrier environment improves the apparent solubility and provides a large surface area for dissolution once release begins [55]. In similar bilosome formulations with hydrophobic drugs, the nanoscale encapsulation produced a 7.1-fold increase in dissolution compared to the drug alone. Thus, bilosomes can markedly improve dasatinib's dissolution profile, ensuring more drug stays in solution for absorption.

The bilosome formulation exhibited a biphasic release pattern: an initial modest release (a small "burst") in the first 1 - 2 hours, followed by a much slower, sustained release over the ensuing hours. In the acidic phase (1 hour, 18.4% and after 2 hours, 29.7% at pH 1.2), only a small fraction of dasatinib (~30%) leached out of the bilosomes. This limited release in gastric-like conditions is intentional and beneficial - it indicates that the majority of the drug remained encapsulated and protected while in the stomach. By contrast, the free drug (dasatinib powder) showed a quicker initial dissolution (71.2% after 2 hours at pH 1.2) due to the high solubility of dasatinib in acidic pH. However, this apparent advantage of the free drug is negated upon entering the intestinal phase: when the medium was shifted to pH 6.8 and 7.4, the free dasatinib precipitated and its dissolved fraction plateaued at a low level (roughly 13-34% by 10 hours). The optimized encapsulated

dasatinib, on the other hand, continued to be released gradually in the intestinal environment, reaching about 99% cumulative release by 10 hours at pH 7.4. This contrast highlights that without the bilosomal carrier, much of the dasatinib cannot maintain solubility at higher pH. In contrast, the bilosomes successfully carried the drug into the intestinal milieu in a solubilized form and then released it over time.

The initial burst release of ~30% from the bilosomes in the acidic environment within 2 hours may be attributed to drug molecules that were loosely associated on the vesicle surface or in near-surface layers, which dissociate quickly once the particles are in contact with release media [59]. After this burst, the remaining drug is released in a controlled, diffusion-driven manner from the interior of the vesicles. The presence of cholesterol and bile salt in the bilayer likely helps modulate the release rate by influencing bilayer fluidity; a stable bilayer can retain the drug and slow its diffusion outwards [73]. The net effect is a sustained-release delivery: even after 10 hours, with most of the drug having been released from the bilosomes (in contrast to the free drug, which essentially releases up to 11.4% at pH 6.8 and 34.4% at pH 7.4 after the initial phase). This prolonged release can be advantageous for maintaining therapeutic drug levels over time from a single dose and could potentially allow for reduced dosing frequency.

Improved Intestinal Permeation and Uptake, bile salts are known permeation enhancers for the intestinal epithelium. By incorporating bile salts into the vesicle, bilosomes can transiently loosen tight junctions or facilitate transcellular uptake, promoting greater transport of dasatinib across the gut wall. Additionally, bilosomes' nano-size and flexible, ultra-deformable membranes allow them to be taken up via M-cells in Peyer's patches of the gut-associated lymphoid tissue [62]. This M-cell uptake can shunt a portion of the absorbed drug into the lymphatic circulation, which is advantageous for highly metabolized drugs like dasatinib by partially bypassing hepatic first-pass metabolism. The net effect is a potential increase in the fraction of the drug that reaches systemic circulation. Indeed, bile-based nanocarriers have demonstrated improved bioavailability in vivo for similar drugs (e.g., a ~2.2-fold increase in oral bioavailability was observed for a bilosomal formulation of a lipophilic drug vs. its free form) [59]. This is in agreement with current study findings.

Another advantage of bilosomes is controlled release and reduced side effects. Formulating dasatinib in bilosomes enables a modulated release profile. The vesicles can be designed to release minimal drug in the stomach (limiting local irritation and preventing wasteful release at low pH) and then gradually release the payload in the intestine. This sustained release can maintain therapeutic levels over an extended period and avoid sharp peaks in concentration. For example, a bilosomal formulation showed negligible drug release in simulated gastric fluid and a prolonged release over 24 hours in intestinal conditions. Such controlled release not only improves absorption timeframes but may also reduce gastrointestinal side effects by avoiding high local drug concentrations in the gut [59].

The MTT assay results show that the optimized dasatinib-loaded bilosomal formulation has strong antiproliferative effects against chronic myeloid leukemia (CML) K562 cells, with an IC $_{50}$  of 1.308 ng/mL. In comparison, the IC $_{50}$  for normal human lymphocytes is 23.044 ng/mL, indicating a 17.6-fold selectivity for cancer cells. This differential cytotoxicity is important for targeted anticancer therapy, as it enhances tumor cell killing while reducing harm to healthy cells.

The increased effectiveness of the bilosomal nanocarrier towards K562 cells can be explained by several interconnected mechanisms. First, the nanocarrier improves drug solubilization and cellular uptake by dispersing dasatinib in an amorphous, molecular form within its matrix. This dispersion, confirmed through analyses like XRD, DSC, and FTIR, enhances water solubility and helps the drug cross cell membranes more efficiently, leading to greater accumulation inside leukemia cells [74]. Additionally, the presence of sodium deoxycholate in the bilayer facilitates bile salt-mediated endocytosis, which boosts the interaction between the vesicles and cell membranes, promoting internalization [75]. Lastly, the bilayer's lipid-polymer structure supports sustained drug release, allowing the drug to remain at cytotoxic concentrations for a longer period, which may contribute to its improved therapeutic effect [76, 77].

The higher IC<sub>50</sub> in normal lymphocytes suggests that the formulation is relatively cytocompatible and mainly targets malignant cells. This selectivity

could be due to differences in tyrosine kinase activity, membrane makeup, or endocytic pathways between cancerous and normal cells, which aligns with previous dasatinib selectivity studies [78-80].

From a translational perspective, these findings support the optimized bilosomal system as a promising delivery platform for dasatinib in hematological malignancies. The observed therapeutic index indicates the potential for dose reduction compared to conventional formulations, which could help mitigate systemic side effects while maintaining antitumor efficacy. Nevertheless, further in vivo pharmacokinetics, biodistribution, and long-term toxicity studies are essential to determine if the in vitro selectivity translates into a meaningful safety margin in clinical settings.

#### CONCLUSION

The optimized dasatinib-loaded bilosomes demonstrated nanoscale uniformity, high drug entrapment, and conversion of the drug to a stable amorphous form, which contributed to enhanced dissolution at intestinal pH. The formulation sustained drug release, minimized gastric loss, and exhibited strong selective cytotoxicity toward CML K562 cells compared to normal lymphocytes. The integration of bile salts, surfactants, cholesterol, and Soluplus within the vesicular matrix provided both physicochemical stability and biopharmaceutical advantages. These results position bilosomes as a robust oral delivery platform with the potential to improve dasatinib's therapeutic index, warranting further in vivo pharmacokinetic and safety evaluations.

#### **CONFLICT OF INTEREST**

The authors declare that there is no conflict of interests regarding the publication of this manuscript.

#### **REFERENCES**

- Chen B-A, Chen R. The role of dasatinib in the management of chronic myeloid leukemia. Drug Des Devel Ther. 2015:773.
- Budha NR, Frymoyer A, Smelick GS, Jin JY, Yago MR, Dresser MJ, et al. Drug Absorption Interactions Between Oral Targeted Anticancer Agents and PPIs: Is pH-Dependent Solubility the Achilles Heel of Targeted Therapy? Clinical Pharmacology and Therapeutics. 2012;92(2):203-213.
- 3. Dasatinib. Profiles of Drug Substances, Excipients and Related Methodology: Elsevier; 2014. p. 205-237.
- Dharani S, Rahman Z, Barakh Ali SF, Afrooz H, Khan MA. Quantitative estimation of phenytoin sodium

- disproportionation in the formulations using vibration spectroscopies and multivariate methodologies. Int J Pharm. 2018;539(1-2):65-74.
- Eley T, Luo FR, Agrawal S, Sanil A, Manning J, Li T, et al. Phase I Study of the Effect of Gastric Acid pH Modulators on the Bioavailability of Oral Dasatinib in Healthy Subjects. The Journal of Clinical Pharmacology. 2009;49(6):700-709.
- Andersson P, Brisander M, Liljebris C, Jesson G, Lennernäs H. Severe Impact of Omeprazole Timing on pH-Sensitive Dasatinib Absorption: Unveiling Substantial Drug– Drug Interaction. The Journal of Clinical Pharmacology. 2024;65(5):588-597.
- Hofmann J, Bartůněk A, Hauser T, Sedmak G, Beránek J, Ryšánek P, et al. Dasatinib anhydrate containing oral formulation improves variability and bioavailability in humans. Leukemia. 2023;37(12):2486-2492.
- 8. He S, Bian J, Shao Q, Zhang Y, Hao X, Luo X, et al. Therapeutic Drug Monitoring and Individualized Medicine of Dasatinib: Focus on Clinical Pharmacokinetics and Pharmacodynamics. Front Pharmacol. 2021;12.
- Lennernäs H, Liljebris C, Brisander M, Jesson G, Andersson P, Larfors G, et al. XS004 Dasatinib (XS004) Improves Variability and Bioavailability in Humans Using Amorphous Solid Dispersion Formulation of Dasatinib with Potential Implications for Its Clinical Use. Blood. 2022;140(Supplement 1):9652-9653.
- Sokač K, Miloloža M, Kučić Grgić D, Žižek K. Polymeric Amorphous Solid Dispersions of Dasatinib: Formulation and Ecotoxicological Assessment. Pharmaceutics. 2024;16(4):551.
- Dharani S, Mohamed EM, Khuroo T, Rahman Z, Khan MA. Formulation Characterization and Pharmacokinetic Evaluation of Amorphous Solid Dispersions of Dasatinib. Pharmaceutics. 2022;14(11):2450.
- Mageshvaran D, Yadav S, Yadav V, Kuche K, Katari O, Jain S. Enhancing oral bioavailability of dasatinib via supersaturable SNEDDS: Investigation of precipitation inhibition and IVIVC through in-vitro lipolysis-permeation model. Int J Pharm. 2025;668:125007.
- Kaul M, Sanin AY, Shi W, Janiak C, Kahlert UD. Nanoformulation of dasatinib cannot overcome therapy resistance of pancreatic cancer cells with low LYN kinase expression. Pharmacol Rep. 2024;76(4):793-806.
- Bahman F, Pittalà V, Haider M, Greish K. Enhanced Anticancer Activity of Nanoformulation of Dasatinib against Triple-Negative Breast Cancer. Journal of Personalized Medicine. 2021;11(6):559.
- Conacher M, Alexander J, Brewer JM. Oral immunisation with peptide and protein antigens by formulation in lipid vesicles incorporating bile salts (bilosomes). Vaccine. 2001;19(20-22):2965-2974.
- Al-mahallawi AM, Abdelbary AA, Aburahma MH.
   Investigating the potential of employing bilosomes as a novel vesicular carrier for transdermal delivery of tenoxicam. Int J Pharm. 2015;485(1-2):329-340.
- Abdel-moneum R, Abdel-Rashid RS. Bile salt stabilized nanovesicles as a promising drug delivery technology: A general overview and future perspectives. J Drug Deliv Sci Technol. 2023;79:104057.
- 18. El-Nabarawi MA, Shamma RN, Farouk F, Nasralla SM. Bilosomes as a novel carrier for the cutaneous delivery for dapsone as a potential treatment of acne: preparation, characterization and in vivo skin deposition assay. J

- Liposome Res. 2019;30(1):1-11.
- Ahmed S, Kassem MA, Sayed S. Bilosomes as Promising Nanovesicular Carriers for Improved Transdermal Delivery: Construction, in vitro Optimization, ex vivo Permeation and in vivo Evaluation. International Journal of Nanomedicine. 2020:Volume 15:9783-9798.
- Palekar-Shanbhag P, Lande S, Chandra R, Rane D. Bilosomes: Superior Vesicular Carriers. Curr Drug Ther. 2020;15(4):312-320
- Ahmad R, Srivastava S, Ghosh S, Khare SK. Phytochemical delivery through nanocarriers: a review. Colloids Surf B Biointerfaces. 2021;197:111389.
- Elebyary T, Sultan A, Abu-Risha S, El Maghraby G. Bilosomes As Oral Drug Delivery Carrier. Journal of Advanced Medical and Pharmaceutical Research. 2024;0(0):49-55.
- 23. Vemuri NM, Ramakrishnan AP. Preformulation. Parenteral Medications: CRC Press; 2019. p. 47-68.
- Ambadas RR, Sunita PP. Validated UV-Spectrophotometric Methods for Determination of Gemifloxacin Mesylate in Pharmaceutical Tablet Dosage Forms. Journal of Chemistry. 2010;7(S1).
- 25. Tsume Y, Takeuchi S, Matsui K, Amidon GE, Amidon GL. In vitro dissolution methodology, mini-Gastrointestinal Simulator (mGIS), predicts better in vivo dissolution of a weak base drug, dasatinib. Eur J Pharm Sci. 2015;76:203-212.
- Donthi M, Saha R, Singhvi G, Dubey S. Dasatinib-Loaded Topical Nano-Emulgel for Rheumatoid Arthritis: Formulation Design and Optimization by QbD, In Vitro, Ex Vivo, and In Vivo Evaluation. Pharmaceutics. 2023;15(3):736.
- Al-Edhari GH, Al Gawhari FJ. Study the Effect of Formulation Variables on Preparation of Nisoldipine Loaded Nano Bilosomes. Iraqi Journal of Pharmaceutical Sciences (P-ISSN 1683 - 3597 E-ISSN 2521 - 3512). 2023;32(Suppl.):271-282.
- Ali SK, Entidhar JA-A. Bilosomes as Soft Nanovesicular Carriers for Ropinirole Hydrochloride: Preparation and In- vitro Characterization. Iraqi Journal of Pharmaceutical Sciences( P-ISSN 1683 - 3597 E-ISSN 2521 - 3512). 2023;32(Suppl.):177-187.
- 29. Zolghadri S, Asad AG, Farzi F, Ghajarzadeh F, Habibi Z, Rahban M, et al. Span 60/Cholesterol Niosomal Formulation as a Suitable Vehicle for Gallic Acid Delivery with Potent In Vitro Antibacterial, Antimelanoma, and Anti-Tyrosinase Activity. Pharmaceuticals. 2023;16(12):1680.
- 30. Kaoud RM, Alwan MH, Amran M, Fawzi HA. Design and optimization of pantoprazole sodium mucoadhesive hydrogel microcapsules for the healing of peptic ulcers. Pharmacia. 2024;71:1-14.
- Lubna Abdalkarim S, Amer Sajjad K. Formulation and Invitro Evaluation of Nanovesicles Bilosomes Loaded with Ketoconazole. Iraqi Journal of Pharmaceutical Sciences. 2025;34(1):156-164.
- 32. Baghdadi RA, Abdalla AN, Abourehab MAS, Tulbah AS. Evaluation of the effects of a dasatinib-containing, selfemulsifying, drug delivery system on HT29 and SW420 human colorectal carcinoma cells, and MCF7 human breast adenocarcinoma cells. Journal of Taibah University Medical Sciences. 2024;19(4):806-815.
- Li C, Li X. Development and Validation of a Method for Determination of Encapsulation Efficiency of CPT-11/ DSPE-mPEG2000 Nanoparticles. Medicinal chemistry. 2016;06(05).
- 34. Khafagy E-S, Almutairy B, Abu Lila A. Tailoring of Novel Bile

- Salt Stabilized Vesicles for Enhanced Transdermal Delivery of Simvastatin: A New Therapeutic Approach against Inflammation. Polymers. 2023;15(3):677.
- 35. Hamed R. Physiological parameters of the gastrointestinal fluid impact the dissolution behavior of the BCS class lla drug valsartan. Pharmaceutical Development and Technology. 2018;23(10):1168-1176.
- 36. Costa P, Sousa Lobo JM. Modeling and comparison of dissolution profiles. Eur J Pharm Sci. 2001;13(2):123-133.
- Siepmann J, Peppas NA. Modeling of drug release from delivery systems based on hydroxypropyl methylcellulose (HPMC). Adv Drug Del Rev. 2012;64:163-174.
- Lee MK, Kim MY, Kim S, Lee J. Cryoprotectants for freeze drying of drug nano-suspensions: Effect of freezing rate. J Pharm Sci. 2009;98(12):4808-4817.
- 39. Roy S, Quiñones R, Matzger AJ. Structural and Physicochemical Aspects of Dasatinib Hydrate and Anhydrate Phases. Crystal Growth and Design. 2012;12(4):2122-2126.
- 40. Sahoo CK, Ramana DV, Sahoo N, Panda KC, Panigrahy UP. Formulation and Evaluation of Immediate release Tablets of Dasatinib using Croscarmelose Sodium. Research Journal of Pharmacy and Technology. 2017;10(3):833.
- 41. Abdul Azeeze MST, Kandasamy S, Palanisamy P, Palanichamy P, Subramania Nainar M. Cocrystallization of Dasatinib with different acids improves the solubility and physicochemical properties: A combined experimental and theoretical studies. Chemical Physics Impact. 2023;7:100247.
- 42. Bellisola G, Cinque G, Vezzalini M, Moratti E, Silvestri G, Redaelli S, et al. Rapid recognition of drug-resistance/ sensitivity in leukemic cells by Fourier transform infrared microspectroscopy and unsupervised hierarchical cluster analysis. The Analyst. 2013;138(14):3934.
- 43. Uzun İ. Methods of determining the degree of crystallinity of polymers with X-ray diffraction: a review. Journal of Polymer Research. 2023;30(10).
- 44. Segal L, Creely JJ, Martin AE, Conrad CM. An Empirical Method for Estimating the Degree of Crystallinity of Native Cellulose Using the X-Ray Diffractometer. Textile Research Journal. 1959;29(10):786-794.
- 45. Ubhe AS. Imaging of Liposomes by Negative Staining Transmission Electron Microscopy and Cryogenic Transmission Electron Microscopy. Methods in Molecular Biology: Springer US; 2023. p. 245-251.
- 46. Cutrignelli A, Sanarica F, Lopalco A, Lopedota A, Laquintana V, Franco M, et al. Dasatinib/HP-β-CD Inclusion Complex Based Aqueous Formulation as a Promising Tool for the Treatment of Paediatric Neuromuscular Disorders. Int J Mol Sci. 2019;20(3):591.
- Oktay AN, Polli JE. Screening of Polymers for Oral Ritonavir Amorphous Solid Dispersions by Film Casting. Pharmaceutics. 2024;16(11):1373.
- 48. Bajerski L, Rossi RC, Dias CL, Bergold AM, Fröehlich PE. Development and Validation of a Discriminating In Vitro Dissolution Method for a Poorly Soluble Drug, Olmesartan Medoxomil: Comparison Between Commercial Tablets. AAPS PharmSciTech. 2010;11(2):637-644.
- Nayak D, Rathnanand M, Tippavajhala VK. Unlocking the Potential of Bilosomes and Modified Bilosomes: a Comprehensive Journey into Advanced Drug Delivery Trends. AAPS PharmSciTech. 2023;24(8).
- Moinuddin, Neekhra S, Ahmad S, Swarnkar SK, Gupta D, Khunteta A, et al. Evaluation of Oral Bioavailability and Invivo Anti-leukemic Potential of Dasatinib Loaded Solid Lipid

- Nanoparticles. International Journal of Pharmaceutical Quality Assurance. 2023;14(03):587-591.
- 51. Ahmed R, Singh R, Kapoor J, Chandra Patra P, Agrawal N, Bhurani D, et al. Attenuated Dose Dasatinib in Newly Diagnosed Chronic Myeloid Leukemia Chronic Phase Patients in India. Clinical Lymphoma Myeloma and Leukemia. 2023;23(2):e71-e77.
- Begum MY, Gudipati PR. Formulation and Evaluation of Dasatinib Loaded Solid Lipid Nanoparticles. International Journal of Pharmacy and Pharmaceutical Sciences. 2018;10(12):14.
- Wang C, Wang M, Chen P, Wang J, Le Y. Dasatinib Nanoemulsion and Nanocrystal for Enhanced Oral Drug Delivery. Pharmaceutics. 2022;14(1):197.
- 54. Levêque D, Becker G, Bilger K, Natarajan-Amé S. Clinical Pharmacokinetics and Pharmacodynamics of Dasatinib. Clin Pharmacokinet. 2020;59(7):849-856.
- 55. Keerikkadu M, Bangera PD, Tippavajhala VK, Rathnanand M. Dasatinib Pharmacokinetics and Advanced Nanocarrier Strategies: from Systemic Limitations to Targeted Success. AAPS PharmSciTech. 2025;26(5).
- Guembe-Michel N, Nguewa P, González-Gaitano G. Soluplus®-Based Pharmaceutical Formulations: Recent Advances in Drug Delivery and Biomedical Applications. Int J Mol Sci. 2025;26(4):1499.
- 57. Bu B, Crowe M, Diao J, Ji B, Li D. Cholesterol suppresses membrane leakage by decreasing water penetrability. Soft Matter. 2018;14(25):5277-5282.
- Garidel P, Hildebrand A, Knauf K, Blume A. Membranolytic Activity of Bile Salts: Influence of Biological Membrane Properties and Composition. Molecules. 2007;12(10):2292-2326
- Ismail A, Teiama M, Magdy B, Sakran W. Development of a Novel Bilosomal System for Improved Oral Bioavailability of Sertraline Hydrochloride: Formulation Design, In Vitro Characterization, and Ex Vivo and In Vivo Studies. AAPS PharmSciTech. 2022;23(6).
- Arafat M. The effect of intestinal bile on the stability of lipid-based vesicular system used as oral drug carriers. Global Drugs and Therapeutics. 2016;2(2).
- Pavlović N, Goločorbin-Kon S, Đanić M, Stanimirov B, Al-Salami H, Stankov K, et al. Bile Acids and Their Derivatives as Potential Modifiers of Drug Release and Pharmacokinetic Profiles. Front Pharmacol. 2018;9.
- 62. Wankhede H, Penumaka SM, Mandal D, Rojatkar S, Gaikwad V, Patil S. Artesunate-loaded bilosomes with enhanced oral bioavailability: in silico and in vitro study against Leishmania donovani promastigotes and in vivo pharmacokinetic assessment in rats. RSC Pharmaceutics. 2025;2(3):541-552.
- 63. Filippov SK, Khusnutdinov R, Murmiliuk A, Inam W, Zakharova LY, Zhang H, et al. Dynamic light scattering and transmission electron microscopy in drug delivery: a roadmap for correct characterization of nanoparticles and interpretation of results. Materials Horizons. 2023;10(12):5354-5370.
- 64. Mahmood Aljamali N. Zetasizer Technique in Biochemistry. Biochemistry and Analytical Biochemistry. 2015;04(02).
- 65. Barbosa JAC, Abdelsadig MSE, Conway BR, Merchant HA. Using zeta potential to study the ionisation behaviour of polymers employed in modified-release dosage forms and estimating their pKa. International Journal of Pharmaceutics: X. 2019;1:100024.
- Zafar A, Alsaidan OA, Imam SS, Yasir M, Alharbi KS, Khalid
   M. Formulation and Evaluation of Moxifloxacin Loaded

- Bilosomes In-Situ Gel: Optimization to Antibacterial Evaluation. Gels. 2022;8(7):418.
- 67. Prüfert F, Fischer F, Leichner C, Zaichik S, Bernkop-Schnürch A. Development and In Vitro Evaluation of Stearic Acid Phosphotyrosine Amide as New Excipient for Zeta Potential Changing Self-Emulsifying Drug Delivery Systems. Pharm Res. 2020;37(4).
- 68. Hancock BC, Zografi G. Characteristics and Significance of the Amorphous State in Pharmaceutical Systems. J Pharm Sci. 1997;86(1):1-12.
- Yu L. Amorphous pharmaceutical solids: preparation, characterization and stabilization. Adv Drug Del Rev. 2001;48(1):27-42.
- Craig DQM. The mechanisms of drug release from solid dispersions in water-soluble polymers. Int J Pharm. 2002;231(2):131-144.
- 71. Abdelwahed W, Degobert G, Fessi H. Freeze-drying of nanocapsules: Impact of annealing on the drying process. Int J Pharm. 2006;324(1):74-82.
- 72. Wang W. Lyophilization and development of solid protein pharmaceuticals. Int J Pharm. 2000;203(1-2):1-60.
- Nsairat H, Khater D, Sayed U, Odeh F, Al Bawab A, Alshaer W. Liposomes: structure, composition, types, and clinical applications. Heliyon. 2022;8(5):e09394.
- 74. shaikh R, Bhattacharya S, Saoji SD. Development, optimization, and characterization of polymeric micelles

- to improve dasatinib oral bioavailability: Hep G2 cell cytotoxicity and in vivo pharmacokinetics for targeted liver cancer therapy. Heliyon. 2024;10(21):e39632.
- Leborgne C, Alimi-Guez D, El Shafey N, van Wittenberghe L, Bigey P, Scherman D, et al. The absorption enhancer sodium deoxycholate promotes high gene transfer in skeletal muscles. Int J Pharm. 2017;523(1):291-299.
- Qin C, Lv Y, Xu C, Li J, Yin L, He W. Lipid-bilayer-coated nanogels allow for sustained release and enhanced internalization. Int J Pharm. 2018;551(1-2):8-13.
- Parveen S, Gupta P, Kumar S, Banerjee M. Lipid polymer hybrid nanoparticles as potent vehicles for drug delivery in cancer therapeutics. Medicine in Drug Discovery. 2023;20:100165.
- Shah NP, Tran C, Lee FY, Chen P, Norris D, Sawyers CL.
   Overriding Imatinib Resistance with a Novel ABL Kinase Inhibitor. Science. 2004;305(5682):399-401.
- Shah NP, Rousselot P, Schiffer C, Rea D, Cortes JE, Milone J, et al. Dasatinib in imatinib-resistant or -intolerant chronicphase, chronic myeloid leukemia patients: 7-year follow-up of study CA180-034. Am J Hematol. 2016;91(9):869-874.
- 80. Bishoyi AK, Nouri S, Hussen A, Bayani A, Khaksari MN, Soleimani Samarkhazan H. Nanotechnology in leukemia therapy: revolutionizing targeted drug delivery and immune modulation. Clin Exp Med. 2025;25(1).